



Gravitational Radiation from Colliding Vacuum Bubbles: Envelope Approximation to Many-Bubble Collisions

Arthur Kosowsky^{1,3} and Michael S. Turner^{1,2,3}

*Departments of Physics¹ and Astronomy & Astrophysics²
Enrico Fermi Institute
The University of Chicago
Chicago, IL 60637-1433*

*³NASA/Fermilab Astrophysics Center
Fermi National Accelerator Laboratory
Batavia, IL 60510-0500*

Abstract. We introduce an approximation to calculate the gravitational radiation produced by the collision of true-vacuum bubbles that is simple enough to allow the simulation of a phase transition by the collision of hundreds of bubbles. This “envelope approximation” neglects the complicated “overlap” regions of colliding bubbles and follows only the evolution of the bubble walls. The approximation accurately reproduces previous results for the gravitational radiation from the collision of two scalar-field vacuum bubbles. Using a bubble nucleation rate given by $\Gamma = \Gamma_0 e^{\beta t}$, we simulate a phase transition by colliding 20 to 200 bubbles; the fraction of vacuum energy released into gravity waves is $E_{\text{GW}}/E_{\text{vac}} = 0.06(H/\beta)^2$ and the peak of the spectrum occurs at $\omega_{\text{max}} = 1.6\beta$ ($H^2 = 8\pi G\rho/3$ is the Hubble constant associated with the false-vacuum phase). The spectrum is very similar to that in the two-bubble case, except that the efficiency of gravity-wave generation is about five times higher, presumably due to the fact that a given bubble collides with many others. Finally, we consider two further “statistical” approximations, where the gravitational radiation is computed as an incoherent sum over individual bubbles weighted by the distribution of bubble sizes. These approximations provide reasonable estimates of the gravitational-wave spectrum with far less computation.



I. Introduction

The cosmic background of gravitational radiation provides a unique probe of the early universe. Unlike electromagnetic radiation, gravity waves propagate virtually unimpeded since the Planck epoch, providing an unmodified record of cosmic events. Possible cosmological sources include the thermal background (the graviton analogue of the microwave background), inflation [1], cosmic strings [2], a pregalactic star population [3], and phase transitions [4]. In particular, strongly first-order phase transitions are among the most promising of all these sources [5]: The energy released in gravitational waves can approach 1% of that in the ambient thermal bath.

In a recent paper we initiated a detailed investigation of gravity wave production from strongly first-order phase transitions by calculating the radiation from two colliding vacuum bubbles [6]. Beginning with a scalar field configuration corresponding to two bubbles nucleated simultaneously and far apart, we used the Klein-Gordon equation to evolve the scalar field for a time τ comparable to the initial bubble separation. (In realistic phase transitions the duration of the transition is comparable to the typical separation of nucleation sites [7].) From the scalar-field configuration, we calculated the stress-energy tensor and, in the linearized gravity approximation, the energy spectrum of radiated gravity waves. The pair of vacuum bubbles radiates efficiently: the fraction of energy that goes into gravity waves is

$$\frac{E_{\text{GW}}}{E_{\text{vac}}} \approx 1.3 \times 10^{-3} \left(\frac{\tau}{H^{-1}} \right)^2, \quad (1)$$

where E_{vac} is the total energy liberated by the two vacuum bubbles, τ is the total time of the bubble evolution, expected to be of order 0.01 to 1 of H^{-1} , and $H^2 = 8\pi G\rho_{\text{vac}}/3$ is the Hubble parameter associated with the vacuum energy. The spectrum of radiation peaks at a frequency

$$\omega_{\text{max}} \simeq 3.8\tau^{-1}. \quad (2)$$

These results imply that vacuum bubble collisions can indeed be potent sources of gravitational radiation. However, our work has its limitations, the foremost being the use of a time cutoff in the simulation to model the end of the phase transition. Specifically, we smoothly ramped the scalar field gradients (the source of gravitational radiation) to zero after a time τ . While such an *ad hoc* prescription greatly simplifies the problem and is probably reasonable, it clearly neglects multi-bubble effects. The motivation for colliding many bubbles is to model more realistically a phase transition.

A direct attack on the many-bubble problem employing scalar-field evolution is numerically infeasible. The two-bubble problem was made tractable by exploiting the $O(2,1)$ symmetry possessed by the space-time of two vacuum bubbles, which makes the scalar field evolution effectively one, rather than two, dimensional. Even the slight generalization to a pair of bubbles nucleated at different times, a situation still having rotational symmetry about the axis connecting the two bubbles, proved nearly impossible. The most general

case of many bubbles in three dimensions has no symmetries and is beyond present computing capabilities. The problem is difficult numerically because of two disparate scales. The bubble wall thickness at nucleation is small compared to the size of the bubble at collision; moreover, the bubble wall becomes thinner due to Lorentz contraction as the bubble expands.

To proceed further requires dispensing with the detailed dynamics of the scalar field. The results of our two-bubble simulations suggested an elegant approximation. The spectrum and amount of gravitational radiation depended only on the gross features of the bubble collisions: the vacuum energy and the size of the bubbles at the end of the phase transition (*i.e.*, the cutoff time). Even though the field dynamics after a bubble collision are quite intricate, the overall contribution to the radiation from the complicated small-scale motions adds incoherently and is subdominant. This prompted us to consider an “envelope approximation”: the bubbles are treated as infinitely thin, and in the regions where bubbles overlap, the bubble wall is completely ignored. Only the envelope of the evolving bubble network is considered. As we shall discuss, the envelope approximation very accurately reproduces our previous results for two colliding bubbles and allows us to model a phase transition with the collision of hundreds of bubbles. When applied to a phase transition where the bubble nucleation rate increases exponentially with time, $\Gamma \propto \exp \beta t$, the fraction of vacuum energy liberated in gravitational waves is found to be

$$\frac{E_{\text{GW}}}{E_{\text{vac}}} \approx 0.06 \left(\frac{H}{\beta} \right)^2, \quad (3)$$

or about five times the efficiency estimated from the collision of two bubbles (for such a nucleation rate, the duration of the transition is $\tau \sim \text{few } \beta$).

The paper is organized as follows. The next Section of this paper describes the envelope approximation, with detailed comparisons to the previous two-bubble results obtained from scalar-field evolution [6]. In Section III we first review some pertinent aspects of bubble nucleation theory [7], and then present our numerical results for the gravitational radiation from large numbers of colliding bubbles. In Section IV, we present another approximation which treats the production of gravitational waves in a statistical sense: as the incoherent sum of radiation from individual bubbles, weighted by the distribution of bubble sizes. Many of the results in Section III can be reproduced by this simple recipe, and with far less computation. We finish with a summary of our work and some concluding remarks. A review of tensor spherical harmonics and some auxiliary formulas used in Section IV are relegated to an Appendix. A summary of the results of this paper and our earlier work [6], as well as the application of our results to cosmological phase transitions, is presented elsewhere [8].

II. Envelope Approximation

(a) Review of vacuum bubbles

We consider a real scalar field φ with a potential possessing two non-degenerate local minima:

$$\mathcal{L} = \frac{1}{2} \partial^\mu \varphi \partial_\mu \varphi - V(\varphi). \quad (4)$$

Throughout we use a metric with signature $(+ - - -)$. The exact form for the potential is not important, but where needed we use

$$V(\varphi) = \frac{\lambda}{8} (\varphi^2 - \varphi_0^2)^2 + \epsilon \lambda \varphi_0^3 (\varphi + \varphi_0). \quad (5)$$

The dimensionless number ϵ measures the degree of symmetry breaking between the two minima near $\pm\varphi_0$. The relative minimum corresponding to $+\varphi_0$ is the “false vacuum,” while the global minimum corresponding to $-\varphi_0$ is the “true vacuum.” The vacuum energy density is defined as the difference in energy density between the true and false vacua; here, $\rho_{\text{vac}} \simeq 2\epsilon\lambda\varphi_0^4$. The height of the potential barrier between the two vacuum states is $\simeq \lambda\varphi_0^4/8$. The relevant features of the potential are that it possesses two inequivalent local minima differing in vacuum energy by ρ_{vac} , and that the height of the barrier between the two minima is large enough so that the false vacuum decays via quantum tunnelling.

Classically, the false-vacuum state is stable, but quantum effects cause its decay to the true-vacuum state. This decay proceeds via the quantum nucleation and expansion of bubbles of the true-vacuum phase which spontaneously appear from the false-vacuum state. Coleman has shown that the bubble with minimum action is $O(4)$ -invariant in Euclidean space [9]; the initial bubble profile is obtained by analytically continuing to Minkowski space and taking the $t = 0$ time slice. The vacuum bubble then evolves according to the Klein-Gordon equation and has $O(3, 1)$ symmetry; i.e., the scalar field φ is a function only of the quantity $t^2 - x^2 - y^2 - z^2$. The energy difference between the true and false vacuum phases creates an effective outward pressure on the bubble wall, causing it to expand with constant acceleration. For our purposes, the important aspects of bubble dynamics are that the expansion speed rapidly approaches the speed of light, and that the false-vacuum energy liberated becomes kinetic and gradient energy of the bubble wall [10].

The bubble’s symmetry allows us to quantify the above statements while deriving a result which will be useful in the envelope approximation. First, the $O(3, 1)$ symmetry immediately implies that the position of the bubble wall is given by

$$\mathbf{x}_{\text{wall}}^2 - t^2 = R_0^2, \quad (6)$$

where R_0 is the initial radius of the bubble and \mathbf{x}_{wall} denotes a fiducial point within the bubble wall. Next, consider the stress-energy tensor associated with the expanding bubble:

$$T_{\mu\nu}(\mathbf{x}, t) = \partial_\mu \varphi \partial_\nu \varphi - g_{\mu\nu} \mathcal{L}. \quad (7)$$

The energy density in the scalar field is given by the time-time component of the stress tensor:

$$T_{00}(\mathbf{x}, t) = \frac{1}{2} \left[\left(\frac{\partial \varphi}{\partial t} \right)^2 + \left(\frac{\partial \varphi}{\partial r} \right)^2 \right] + V(\varphi) \quad (8)$$

where we have used the spherical symmetry of the bubble solution. The bubble's $O(3, 1)$ symmetry can be used to write the energy of the bubble wall at any time t as

$$E(t) \approx 4\pi \int dr r^2 \left[\frac{1}{2} \left(\frac{\partial \varphi}{\partial t} \right)^2 + \frac{1}{2} \left(\frac{\partial \varphi}{\partial r} \right)^2 \right] \quad (9a)$$

$$= 2\pi \int_0^\infty ds \left(\frac{d\varphi}{ds} \right)^2 \left[\frac{t^2 \sqrt{(s^2 + t^2)}}{s} + \frac{\sqrt{(s^2 + t^2)^3}}{s} \right], \quad (9b)$$

where $s = \sqrt{r^2 - t^2}$ and $\varphi(s) = \varphi(r, t = 0)$ is the profile of the initial bubble solution. Note that for $r^2 < t^2$, $d\varphi/ds = 0$ so the integral is zero. The two terms represent the kinetic and gradient energy of the bubble wall. We neglect the potential energy term inside the bubble wall as it rapidly becomes unimportant as the bubble wall gets thinner; we have not included the false-vacuum energy outside the bubble, as we are only interested in the energy liberated by the bubble. In Fig. 1, the kinetic and gradient energy for a bubble are shown as a function of time. After a short time, the energies become equal; each is half of $4\pi\rho_{\text{vac}}t^3/3$, the total vacuum energy liberated by the bubble. From Eq. (9b) it is simple to see that gradient and kinetic energies are equal and increase as t^3 for $t \gg R_0$: $d\varphi/ds$ is only nonzero when s is close to R_0 ; when $t \gg R_0$ each term in the integrand approaches $(d\varphi/ds)^2 t^3/s$.

(b) Envelope approximation

As in our previous paper [6], we compute gravity-wave production in the linearized gravity approximation, valid for bubble sizes less than H^{-1} (recall $H^2 = 8\pi G\rho_{\text{vac}}/3$). The energy radiated in gravitational waves can be expressed in terms of the Fourier transform of the spatial components of the scalar-field stress-energy tensor. Further, in computing $T_{ij}(\mathbf{k}, \omega)$ we may neglect the $\mathcal{L}g_{ij}$ piece as it is a pure trace and does not act as a source for gravitational radiation. Thus the fundamental quantity is

$$T_{ij}(\hat{\mathbf{k}}, \omega) = \frac{1}{2\pi} \int_0^\infty dt e^{i\omega t} \int d^3x \partial_i \varphi \partial_j \varphi e^{-i\omega \hat{\mathbf{k}} \cdot \mathbf{x}} \quad (10)$$

where $\hat{\mathbf{k}}$ is a unit wave-vector. As before, we adopt Weinberg's unusual normalization convention for the Fourier transform [11]. The scalar-field configuration of interest is that of many colliding vacuum bubbles. In the envelope approximation we assume that the overlap regions where bubbles have expanded into one another do not contribute substantially to the gravitational radiation, and exclude these regions from the spatial integration (see Fig. 2). We can then break up the integral into integration regions, one surrounding each

nucleation site and extending out to the bubble radius. Equation (10) becomes

$$T_{ij}(\hat{\mathbf{k}}, \omega) \approx \frac{1}{2\pi} \int_0^\infty dt e^{i\omega t} \left[\sum_{n=1}^N \int_{S_n} d\Omega' e^{-i\omega \hat{\mathbf{k}} \cdot \mathbf{x}} \int dr' r'^2 \partial_i \varphi \partial_j \varphi \right] \quad (11)$$

where N is the number of bubbles, S_n is the portion of the surface of bubble n that remains uncollided at time t , and the primed spherical coordinates are chosen independently around the center of each bubble. We have also assumed that the wall thickness is small compared to ω^{-1} : $\omega \Delta r \ll 1$. This means $e^{-i\omega \hat{\mathbf{k}} \cdot \mathbf{x}}$ is essentially constant across the bubble wall and can be factored out of the r -integral. In practice, for the frequencies of interest, this is always an excellent approximation.

Next we use the fact that each bubble is spherically symmetric around its center, so that φ is independent of the angular variables. Dropping the primes for notational convenience, the stress tensor components become

$$T_{ij}(\hat{\mathbf{k}}, \omega) = \frac{1}{2\pi} \int_0^\infty dt e^{i\omega t} \left[\sum_{n=1}^N e^{-i\omega \hat{\mathbf{k}} \cdot \mathbf{x}_n} \int_{S_n} d\Omega e^{-i\omega \hat{\mathbf{k}} \cdot \mathbf{x}} \hat{x}_i \hat{x}_j \int dr r^2 \left(\frac{\partial \varphi}{\partial r} \right)^2 \right] \quad (12)$$

where \mathbf{x}_n is the nucleation site of the n th bubble and \hat{x}_i is the i th component of a unit vector pointing from \mathbf{x}_n in the direction $d\Omega$:

$$\hat{x} = \sin \theta \cos \phi, \quad \hat{y} = \sin \theta \sin \phi, \quad \hat{z} = \cos \theta.$$

Above we showed that the kinetic and gradient energy associated with a bubble wall are equal after a small amount of bubble expansion. Using Eq. (9a), for each bubble we have

$$4\pi \int dr r^2 \left(\frac{\partial \varphi}{\partial r} \right)^2 \approx \frac{4\pi}{3} R^3 \rho_{\text{vac}} \quad (13)$$

where the bubble radius $R(t) \approx t$. This is a very good approximation by the time a bubble has doubled in size; cf. Fig. 1. Substituting $t^3 \rho_{\text{vac}}/3$ for the radial integral in Eq. (12) leads to

$$T_{ij}(\hat{\mathbf{k}}, \omega) = \frac{\rho_{\text{vac}}}{6\pi} \int_0^\infty dt e^{i\omega t} \left[\sum_{n=1}^N (t - t_n)^3 e^{-i\omega \hat{\mathbf{k}} \cdot \mathbf{x}_n} \int_{S_n} d\Omega e^{-i\omega \hat{\mathbf{k}} \cdot \mathbf{x}} \hat{x}_i \hat{x}_j \right] \quad (14)$$

where t_n is the nucleation time of bubble n .

The total energy radiated in gravity waves is given in terms of $T_{ij}(\hat{\mathbf{k}}, \omega)$ by [11]

$$\frac{dE}{d\omega d\Omega} = 2G\omega^2 \Lambda_{ij,lm}(\hat{\mathbf{k}}) T_{ij}^*(\hat{\mathbf{k}}, \omega) T_{lm}(\hat{\mathbf{k}}, \omega) \quad (15)$$

where $\Lambda_{ij,lm}$ is the projection tensor for gravity waves,

$$\begin{aligned} \Lambda_{ij,lm}(\hat{\mathbf{k}}) \equiv & \delta_{il} \delta_{jm} - 2\hat{\mathbf{k}}_j \hat{\mathbf{k}}_m \delta_{il} + \frac{1}{2} \hat{\mathbf{k}}_i \hat{\mathbf{k}}_j \hat{\mathbf{k}}_l \hat{\mathbf{k}}_m \\ & - \frac{1}{2} \delta_{ij} \delta_{lm} + \frac{1}{2} \delta_{ij} \hat{\mathbf{k}}_l \hat{\mathbf{k}}_m + \frac{1}{2} \delta_{lm} \hat{\mathbf{k}}_i \hat{\mathbf{k}}_j. \end{aligned} \quad (16)$$

(c) *Scaling properties*

From Eqs. (14) and (15), two important scaling relations are evident. First, the total radiated energy is explicitly proportional to ρ_{vac}^2 , just as we found previously in the two-bubble case [6]. Second, since the bubbles expand at essentially the speed of light and to a good approximation have zero thickness and zero initial size, the problem has no intrinsic length/time scale. Making the transformation $t \rightarrow \gamma t$, $\mathbf{x} \rightarrow \gamma \mathbf{x}$, we find the following scaling properties:

$$\omega \rightarrow \frac{\omega}{\gamma}; \quad (17a)$$

$$\frac{dE}{d\omega d\Omega} \rightarrow \gamma^6 \frac{dE}{d\omega d\Omega}; \quad (17b)$$

$$E_{\text{GW}} \rightarrow \gamma^5 E_{\text{GW}}. \quad (17c)$$

The length/time scale is set by the average separation between bubble nucleation sites.

Equations (17) show that the total energy radiated from a volume containing a fixed number of bubbles will vary with the fifth power of the mean bubble separation. As we will show in the next Section, these scalings can also be expressed in terms of the bubble nucleation rate, since the typical separation of nucleation sites is determined by the nucleation rate. For the two-bubble case, the above scalings were found previously to hold to very good accuracy [6], where the relevant scale is the total evolution time. These scalings have great practical importance as they allow us to apply the results of a single numerical simulation to any phase transition with a bubble nucleation rate of the same functional form. In particular, we shall use the functional form $\Gamma \propto e^{\beta t}$ —a nucleation rate that increases exponentially with time—in which case the length/time scale is just β^{-1} .

(d) *Two bubbles, quadrupole approximation*

In order to determine the accuracy of the envelope approximation, we compare the results it gives for two bubbles to the results calculated previously with the exact scalar field evolution [6]. As a warm-up, we begin with the conventional “quadrupole approximation,” corresponding to the limit $\mathbf{k} \cdot \mathbf{x} \rightarrow 0$:

$$T_{ij}(\hat{\mathbf{k}}, \omega) = \frac{\rho_{\text{vac}}}{6\pi} \int_0^\infty dt e^{i\omega t} \left[\sum_{n=1}^N (t - t_n)^3 \int_{S_n} d\Omega \hat{\mathbf{x}}_i \hat{\mathbf{x}}_j \right]. \quad (18)$$

Note that because our source is not small compared to the wavelength of the radiation, this approximation does *not* correspond to the quadrupole term in the multipole expansion; see Ref. [6] for detailed elucidation of this point. The quadrupole approximation simplifies the requires calculations, and in the limit $\omega \rightarrow 0$ gives the correct result; thus we use it as a starting point for our comparisons.

Consider two bubbles of negligible initial size nucleated simultaneously at $t = 0$ on the z -axis at $\pm d/2$. The bubbles will first “kiss” at $t = d/2$. Define $\cos \alpha = d/2t$ for $t > d/2$

and $\alpha = 0$ for $t < d/2$; α is the angle excluded from the angular integration because of bubble overlap in the envelope approximation. Then

$$T_{ij} = \frac{\rho_{\text{vac}}}{6} \int_0^\infty dt e^{i\omega t} t^3 \left[\int_0^{\pi-\alpha} d\theta \sin\theta \int_0^{2\pi} d\phi \hat{x}_i \hat{x}_j + \int_\alpha^\pi d\theta \sin\theta \int_0^{2\pi} d\phi \hat{x}_i \hat{x}_j \right]. \quad (19)$$

Using the spherical coordinates defined in Eq. (11),

$$T_{xx} = T_{yy} = \frac{\rho_{\text{vac}}}{3} \int_{d/2}^\infty dt e^{i\omega t} \left(\frac{2}{3} t^3 + \frac{d}{2} t^2 - \frac{d^3}{24} \right) C(t) \quad (20a)$$

and

$$T_{zz} = \frac{2\rho_{\text{vac}}}{9} \int_{d/2}^\infty dt e^{i\omega t} \left(t^3 + \frac{d^3}{8} \right) C(t), \quad (20b)$$

where we have included a time cutoff function $C(t)$ which decreases smoothly from 1 to 0 on a time scale $\tau \sim \mathcal{O}(d)$. As mentioned earlier, the cutoff was introduced in our previous two-bubble calculations to model the completion of the phase transition; $C(t)$ is discussed in detail in Ref. [6].

Rotational symmetry around the z -axis implies the off-diagonal components of the stress tensor are zero, and T_{ij} must be of the form

$$T_{ij} = D(\omega) \delta_{ij} + \Delta(\omega) \delta_{iz} \delta_{jz}. \quad (21)$$

The first term, being a pure trace, does not contribute to gravitational radiation. The second term is

$$\begin{aligned} \Delta(\omega) &\equiv T_{zz} - \frac{1}{2}(T_{xx} + T_{yy}) \\ &= \frac{\rho_{\text{vac}}}{3} \int_{d/2}^\infty dt e^{i\omega t} \left(\frac{d^3}{8} - \frac{d}{2} t^2 \right) C(t). \end{aligned} \quad (22)$$

Substitution into Eq. (15) gives

$$\frac{dE}{d\omega d\Omega} = G\omega^2 |\Delta(\omega)|^2 \sin^4 \theta; \quad \frac{dE}{d\omega} = \frac{32\pi}{15} G\omega^2 |\Delta(\omega)|^2. \quad (23)$$

The comparison of the envelope approximation with the previous calculations using scalar-field evolution is shown in Fig. 3. (For reference, in the scalar-field evolution case we used $\tau/d = 1.2$ and a gaussian roll-off in the final 10% of the evolution time for $C(t)$; see [6].) The features of the spectrum are reproduced remarkably well. The overall normalization of the envelope approximation is high by 20 percent. It may seem strange that the total power radiated is higher from an approximation which neglects a chunk of the source. However, when two bubbles collide, a reflected wave begins to propagate outward from the point of collision. This wave takes the approximate shape that the colliding portion of the bubbles would have had they not collided. By neglecting the interaction

region, we actually make a given bubble *less* spherical, and hence increase the amount of radiation.

(e) *Two bubbles, full linearized gravity approximation*

For two bubbles in the full linearized-gravity approximation, we can derive formulas analogous to those used with the scalar field evolution. As in the quadrupole case, let the bubbles be nucleated at $t = 0$ and at $z = \pm d/2$, with $\tau/d = 1.2$ and the same time cutoff function. The problem possesses rotational symmetry about the z -axis, so without loss of generality we take $k_y = 0$, $k_x = \omega \sin \xi$, $k_z = \omega \cos \xi$. Using the same conventions as in the quadrupole case, the stress-energy tensor components are given by

$$T_{ij}(\hat{\mathbf{k}}, \omega) = \frac{\rho_{\text{vac}}}{6\pi} \int_0^\infty dt e^{i\omega t} t^3 C(t) \left[e^{-ik_z d/2} \int_0^{\pi-\alpha} d\theta \sin \theta \int_0^{2\pi} d\phi e^{-i\mathbf{k}\cdot\mathbf{x}} \hat{\mathbf{x}}_i \hat{\mathbf{x}}_j \right. \\ \left. + e^{ik_z d/2} \int_\alpha^\pi d\theta \sin \theta \int_0^{2\pi} d\phi e^{-i\mathbf{k}\cdot\mathbf{x}} \hat{\mathbf{x}}_i \hat{\mathbf{x}}_j \right]. \quad (24)$$

The ϕ integral can be done explicitly using the identity

$$\int_{-\pi}^\pi e^{i\beta \cos x} \cos nx \, dx = 2i^n \pi J_n(\beta), \quad (25)$$

resulting in the following expressions:

$$T_{xx}(\hat{\mathbf{k}}, \omega) = \frac{\rho_{\text{vac}}}{3} \int_0^\infty dt e^{i\omega t} t^3 C(t) \int_0^{\pi-\alpha} d\theta \sin^3 \theta \cos(k_z t \cos \theta + \frac{1}{2} k_z d) \\ \times [J_0(k_x t \sin \theta) - J_2(k_x t \sin \theta)], \quad (26a)$$

$$T_{yy}(\hat{\mathbf{k}}, \omega) = \frac{\rho_{\text{vac}}}{3} \int_0^\infty dt e^{i\omega t} t^3 C(t) \int_0^{\pi-\alpha} d\theta \sin^3 \theta \cos(k_z t \cos \theta + \frac{1}{2} k_z d) \\ \times [J_0(k_x t \sin \theta) + J_2(k_x t \sin \theta)], \quad (26b)$$

$$T_{zz}(\hat{\mathbf{k}}, \omega) = \frac{2\rho_{\text{vac}}}{3} \int_0^\infty dt e^{i\omega t} t^3 C(t) \int_0^{\pi-\alpha} d\theta \sin \theta \cos^2 \theta \\ \times \cos(k_z t \cos \theta + \frac{1}{2} k_z d) J_0(k_x t \sin \theta), \quad (26c)$$

$$T_{xz}(\hat{\mathbf{k}}, \omega) = \frac{-2\rho_{\text{vac}}}{3} \int_0^\infty dt e^{i\omega t} t^3 C(t) \int_0^{\pi-\alpha} d\theta \sin^2 \theta \cos \theta \\ \times \sin(k_z t \cos \theta + \frac{1}{2} k_z d) J_1(k_x t \sin \theta). \quad (26d)$$

Note that $T_{xy} = T_{yz} = 0$. The energy radiated in gravity waves simplifies to

$$\frac{dE}{d\omega d\Omega} = G\omega^2 \left| T_{zz}(\hat{\mathbf{k}}, \omega) \sin^2 \xi + T_{xx}(\hat{\mathbf{k}}, \omega) \cos^2 \xi \right. \\ \left. - T_{yy}(\hat{\mathbf{k}}, \omega) - 2T_{xz}(\hat{\mathbf{k}}, \omega) \sin \xi \cos \xi \right|^2. \quad (27)$$

In Fig. 4 we compare the envelope approximation with the previous results using scalar-field evolution. As in the quadrupole case, the agreement is excellent, with the envelope approximation power being slightly greater.

III. Numerical Methods and Results

(a) Bubble nucleation [7]

The envelope approximation closely reproduces the gravitational radiation from a two-bubble collision, even showing the same features in the spectrum. This gives us confidence to apply the approximation to the situation where many bubbles are nucleated, collide, and transform all of space to the true vacuum. In a phase transition the bubble nucleation rate per unit volume, Γ , is in general a function of time, due to its dependence upon the temperature of the universe or the evolution of other fields. Since very generally Γ is the exponential of some action, we write it as

$$\Gamma(t) = C e^{-A(t)}. \quad (28)$$

The prefactor C is expected to be of the order of \mathcal{M}^4 , where \mathcal{M} is the mass or energy scale characterizing the transition. The tunnelling action $A(t)$ must be greater than order unity; otherwise, the transition will not proceed via bubble nucleation but through spinodal decomposition, because of the very small potential barrier between the false and true vacuum states. (For the form of the potential in Eq. (5), $A \gg 1$ obtains for $\epsilon \ll 1$.) The fact that the nucleation rate varies with time is crucial to the completion of the phase transition; moreover, how fast it varies with time determines the distribution of bubble sizes. As a rough rule, the phase transition completes when one bubble is nucleated per Hubble volume per Hubble time, *i.e.* when $\Gamma(t)/H^4 \sim 1$. Denote the completion time, about which we shall be more specific, by t_* . Expanding $A(t)$ about t_* gives

$$A(t) \approx A_* - \beta(t - t_*), \quad \beta = - \left(\frac{d \ln \Gamma}{dt} \right) \Big|_{t_*} = \left(\frac{\partial A}{\partial t} \right) \Big|_{t_*}, \quad (29)$$

where $A_* \equiv A(t_*)$. In any sensible model, $\beta > 0$; *i.e.*, the nucleation rate grows with time. As we shall see, β^{-1} sets the time/length scale for the phase transition.

We now derive some important results for the exponential nucleation rate. The fundamental quantity is $p(t)$, the probability that a given point in space remains in the false vacuum at time t . It is given by $p(t) = \exp[-I(t)]$, where $I(t)$ is the expected fraction of space occupied by true-vacuum bubbles at time t , without regard to bubble overlap:

$$I(t) = \frac{4\pi}{3} \int_{t_0}^t dt' \Gamma(t') a^3(t') r^3(t, t'), \quad (30a)$$

where $a(t)$ is the cosmic scale factor, $r(t, t')$ is the coordinate radius at time t of a bubble nucleated at time t' , and t_0 is the time at which the phase transition begins [12]. For

simplicity and consistency with our previous neglect of the expansion of the universe, we take a to be constant and $ar(t, t') = t - t'$. The neglect of the expansion is justified provided the duration of the transition is less than H^{-1} . The second assumption implies that bubbles expand to a size far greater than that when nucleated, which is well-justified in the cases of interest. Taking $t_0 \rightarrow -\infty$ with little error, it follows that

$$I(t) \approx \frac{8\pi}{\beta^4} \Gamma(t). \quad (30b)$$

Then the false-vacuum fraction is given by

$$p(t) = e^{-I(t)} \approx e^{-8\pi\Gamma(t)/\beta^4} \quad (31)$$

where the exponentiation accounts for the bubble overlap. From $p(t)$ we can compute the duration of the phase transition and distribution of bubble sizes. The start and end of the transition are somewhat difficult to define precisely, but this ambiguity is not important. To be specific, we can define the start of the transition to be the time t_m when $p(t_m) = e^{-m} \approx 1$, i.e., $m \ll 1$. Similarly, we define the end of the transition to be the time t_* when $p(t_*) = e^{-M} \approx 0$, i.e. $M \gg 1$. The duration of the transition is thus

$$\delta t \equiv t_* - t_m = \ln \left(\frac{M}{m} \right) \beta^{-1}, \quad (32)$$

and depends only logarithmically upon the precise definition of the start and end of the phase transition. Note that the duration of the phase transition is set by β^{-1} , and that for consistency our neglect of the expansion of the universe requires the duration to be less than a Hubble time: $\beta^{-1} \ll H^{-1}$.

The density (per unit volume) of bubbles of a given radius r at time t is related to $\Gamma(t)$ and $p(t)$ by

$$\begin{aligned} \left(\frac{dn}{dr} \right)_t &= p(t') \Gamma(t') \Big|_{t'=t-r} \\ &\approx \frac{\beta^4 I(t)}{8\pi} \exp[-I(t)e^{-\beta r} - \beta r]. \end{aligned} \quad (33)$$

The distribution of bubble sizes attains its maximum at

$$\bar{r}(t) = \frac{1}{\beta} \ln I(t) \quad (34)$$

and has a width of order β^{-1} . In discussing gravitational wave production it is more appropriate to examine the energy-weighted bubble distribution. Since the energy carried in the expanding wall of a bubble is proportional to its volume, this distribution is obtained by multiplying dn/dr by r^3 :

$$\left(\frac{dn_E}{dr} \right)_t = \frac{\beta^4 I(t) \rho_{\text{vac}}}{6} r^3 \exp[-I(t)e^{-\beta r} - \beta r]. \quad (35)$$

This distribution is peaked at a radius twice as large as dn/dr (see Fig. 5).

Finally, how is the key parameter β related to H and \mathcal{M} ? Since H^{-1} sets the scale for all time evolution in the universe, on very general grounds we expect $\beta = -(\partial A/\partial t)_{t_*}$ to be of the order of $A(t_*)/H^{-1}$, or $\beta^{-1} \sim H^{-1}/A_*$. If the transition is to proceed via vacuum bubbles, A_* must be much greater than one, so the assumption that the transition is “fast”, $\beta^{-1} \ll H^{-1}$, should generally be satisfied. We can also estimate A_* : $\Gamma(t_*) = \mathcal{M}^4 e^{-A_*} \sim H^4 \sim \mathcal{M}^8/m_{\text{Pl}}^4$, which implies that A_* should be of order $\ln(m_{\text{Pl}}/\mathcal{M})$.

(b) Numerical results

In the previous sub-section we have motivated the use of an exponential nucleation rate; specifically,

$$\Gamma(t) = \Gamma_0 e^{\beta t}. \quad (36)$$

As we have discussed, β^{-1} sets the fundamental time/length scale: both the duration of the transition and the typical bubble size are of order a few β^{-1} . We use a spherical volume, and choose Γ_0 so that on average, the desired number of bubbles are nucleated in the sample volume. Our main calculations (see below) use a sample volume with a radius of $4.46\beta^{-1}$ and $\Gamma_0 = 1.38 \times 10^{-3}\beta^4$. These parameters yield an average of around thirty bubbles in the sample volume. For our five different nucleation runs, the time at which the phase transition completes varied from $5\beta^{-1}$ to $6\beta^{-1}$, with an average of $5.63\beta^{-1}$. (We use the time when the last bubble is nucleated in the sample volume as the completion time of the phase transition.)

A “nucleation run” proceeds as follows. For each time step we: (1) Perform a Monte Carlo integration over the sample volume to determine the fraction still in the false-vacuum state. This takes into account all true-vacuum bubbles nucleated prior to the time step. (2) Multiply $\Gamma(t)$ by the sample volume still in the false vacuum and length of the time step to get the mean number of bubbles nucleated during the time step. (3) Use this mean number to generate a Poisson-distributed random number of bubbles nucleated during the time step. (4) Nucleate this number of bubbles at random points in the false-vacuum and during the time step. We choose the time step so that the time from the first nucleation to the disappearance of all the false vacuum is around 100 time steps.

The initial conditions for the simulations consist of nucleation sites and times within the spherical volume produced by the above procedure. We use a spherical boundary to minimize edge effects. We also utilize reflecting boundaries: When a bubble expands into the boundary, the part of the bubble that passes the boundary is ignored. In the context of the envelope approximation, this is equivalent to having another bubble outside the boundary expand into the bubble in question, with their first contact occurring at the boundary surface. Note that in the envelope approximation, reflecting and absorbing boundaries are equivalent.

The aim of the simulation is to numerically evaluate Eq. (14) for the stress-tensor components $T_{ij}(\vec{k}, \omega)$ for the given initial conditions, and then Eq. (15) for the spectrum

of gravitational radiation produced. Note no radiation is produced before the first bubble collision occurs or after the transition to true vacuum has completed; thus these are the limits for the time integration. Our numerical calculations proceed as follows: First we choose values for ω and the direction $\hat{\mathbf{k}}$. Then we numerically evaluate the integrals in Eq. (14). The time partition is chosen for around 100 time steps, and the angular partition is chosen to give 20 divisions per wavelength at a given radiation frequency. These partitions produce numerical integration results accurate to within 5% at all frequencies of interest.

Since bubble nucleation is an inherently random process, we want to find the power spectrum of gravity waves, averaged over many different nucleation realizations. We have calculated the radiation from five simulations averaging 30 bubbles each, ranging from 17 to 38 bubbles. Figure 6 shows a cross-sectional slice through the equator of the spherical volume for one nucleation run; the combined bubble envelope, which is the radiation source, is shown at several times. For each simulation, we have computed the radiation in six directions, along the $\pm x$, $\pm y$, and $\pm z$ axes. The results for $dE/d\omega d\Omega$ for several representative directions are displayed in Fig. 7.

Several features are evident from these results. First, all of the spectra peak at a characteristic frequency which roughly corresponds to the size of the largest bubbles at the end of the transition. Second, the power generally increases as the number of bubbles in a given volume decreases, as we expect ($dE/d\omega d\Omega$ should vary as $N^{-5/3}$). Finally and most obviously, the various runs and directions of observations have very large fluctuations in both total power and spectrum shape. This is because with the relatively small number of bubbles, the source has large inhomogeneities on the scale of the sample volume. One direction in one simulation (*i.e.*, one out of 30 probes of $dE/d\omega d\Omega$) exhibits a “beaming” effect, with ten to a hundred times more power than average at frequencies higher than several times the peak frequency.

Figure 8 shows the power radiated in gravity waves per octave averaged over all five simulations, six directions per simulation (excluding the one anomalously “hot” direction); the error bars indicate the statistical deviation of the mean. On the same plot we show our previous results for the collision of two scalar-field bubbles [6]. Recall the previous results depend upon the cutoff time τ , which corresponds to the duration of the transition. To compare the old results with the present ones, we set $\tau = 3.2/\beta$. We choose this value for τ because it is the mean energy-weighted bubble size at the end of the phase transition (*cf.* Fig. 5). We have divided our results by the total vacuum energy of the sample volume, so the results shown are the fraction of false-vacuum energy liberated in gravitational waves per octave. The two-bubble and many-bubble results are remarkably similar: behavior at high and low frequencies is almost identical, and the peaks are at almost the same frequency. The overall normalization of the many-bubble case is higher, by a factor of five or so on the low-frequency side and by an order of magnitude on the high-frequency side. This increase is not unexpected: In the many-bubble case, each bubble collides with many

others, increasing its total radiation. The excess of high frequency power also makes sense, since the size of a given bubble roughly determines the frequency at which it radiates. In the two-bubble case, both bubbles are the same size; in the many-bubble case, smaller bubbles are nucleated late and increase the high-frequency power.

The total fraction of vacuum energy released in gravitational radiation is computed by integrating $dE/d\omega$ and dividing by the total vacuum energy released:

$$\frac{E_{\text{GW}}}{E_{\text{vac}}} = 0.50 \frac{G\rho_{\text{vac}}}{\beta^2} = 6.0 \times 10^{-2} \left(\frac{H}{\beta}\right)^2. \quad (37)$$

The peak of the energy spectrum is given by $\omega_{\text{max}} \approx 1.6\beta$. We note that the characteristic frequency defined by the maximum of the energy-weighted bubble distribution $\omega_* = 2\pi/\bar{r}_E \approx 1.6\beta$ coincides with ω_{max} . Comparing these results with our previous two-bubble results (taking $\tau = 3.2/\beta$), the peak of the spectrum occurs at the same frequency, while the total fraction of energy liberated in gravity waves is about a factor of five larger.

To verify that our results are not dominated by edge effects, we ran one large calculation in a spherical sample volume with twice the radius of the above simulation and the same nucleation rate, 180 bubbles in all. The radiation spectrum $dE/d\omega$, integrated over the six observation directions, is plotted in Fig. 8. The shape of the spectrum is close to the average of the previous cases, and $E_{\text{GW}}/E_{\text{vac}} = 0.47G\rho_{\text{vac}}/\beta^2$. The close correspondence (only 5% difference) with our smaller simulations demonstrates that edge effects are not important.

IV. Statistical Bubble Approximation

Now we discuss two approximations for computing the gravitational-wave production from the collision of many bubbles as the incoherent sum of the radiation from individual bubbles. To this end, we use the multipole-radiation formalism and the envelope approximation applied to a typical bubble of size R , and integrate over the distribution of bubble sizes. The advantage of such an approach is ease of computation: We can immediately calculate the radiation spectrum for a given nucleation rate, without recourse to a many-bubble simulation. Of course, this approach neglects coherent effects between bubbles and is less accurate than our calculations of the previous Section, but as we shall see it still gives a reasonable estimate of the gravitational radiation produced.

Consider a single expanding bubble in a sea of bubbles. In the envelope approximation, when the bubble in question begins interacting with other bubbles, portions of the bubble surface are “eaten.” Neglecting the interaction regions between bubbles, the stress tensor for what remains of the bubble is

$$T_{ij}(\mathbf{x}, t) = \hat{\mathbf{x}}_i \hat{\mathbf{x}}_j \left(\frac{\partial \varphi(r, t)}{\partial r} \right)^2 \Theta(\Omega, t) \quad (38)$$

where Θ is defined as

$$\Theta(\Omega, t) = \begin{cases} 1, & \text{surface in direction } \Omega \text{ remains uncollided} \\ 0, & \text{otherwise.} \end{cases} \quad (39)$$

When the bubble wall has completely disappeared due to collisions with other bubbles, the function Θ is zero. This means that an individual bubble can be treated as a source that is bounded in space and time: $\Delta t, \Delta x \lesssim \mathcal{O}(\tau)$, where τ is the duration of the phase transition. The size and energy density of a given bubble at any time during a phase transition is known; the function Θ varies from bubble to bubble. Our statistical approximation boils down to estimating an “average” $\Theta(\Omega, t)$.

(a) *Multipole-radiation formalism*

Using the tensor spherical harmonics presented in the Appendix, we can expand the transverse-traceless part of the metric perturbation (i.e., the gravity wave piece) in the far field zone ($r \gg \tau$) as follows [13]:

$$h_{ij}^{TT}(t, \mathbf{r}) = \frac{G}{r} \sum_{l=2}^{\infty} \sum_{m=-l}^l \left[\frac{d^l}{dt^l} I^{lm}(t-r) \mathbb{T}_{ij}^{E2,lm}(\Omega) + \frac{d^l}{dt^l} S^{lm}(t-r) \mathbb{T}_{ij}^{B2,lm}(\Omega) \right], \quad (40)$$

where the I^{lm} and the S^{lm} are the “mass” and “current” multipole moments of the source, respectively, defined by

$$\begin{aligned} \frac{d^l}{dt^l} I^{lm}(t) &= 8(-i)^{l+2} \int r'^2 dr' d\Omega' dt' d\omega e^{-i\omega(t-t')} \tau_{pq}(t', r', \Omega') \\ &\times \left[a_{-2}(l) \mathbb{T}_{pq}^{2l-2,lm}(\Omega')^* j_{l-2}(\omega r') - a_0(l) \mathbb{T}_{pq}^{2l,lm}(\Omega')^* j_l(\omega r') \right. \\ &\quad \left. + a_2(l) \mathbb{T}_{pq}^{2l+2,lm}(\Omega')^* j_{l+2}(\omega r') \right], \quad (41a) \end{aligned}$$

$$\begin{aligned} \frac{d^l}{dt^l} S^{lm}(t) &= 8(-i)^{l+2} \int r'^2 dr' d\Omega' dt' d\omega e^{-i\omega(t-t')} \tau_{pq}(t', r', \Omega') \\ &\times \left[a_{-1}(l) \mathbb{T}_{pq}^{2l-1,lm}(\Omega')^* j_{l-1}(\omega r') - a_1(l) \mathbb{T}_{pq}^{2l+1,lm}(\Omega')^* j_{l+1}(\omega r') \right]. \quad (41b) \end{aligned}$$

The tensors $\mathbb{T}^{2i,lm}(\Omega)$ and the coefficients a_i are given by Equations (A.2) and (A.4) in the Appendix, j_l is the spherical Bessel function of order l , p and q are indices of the tensor components, and τ_{pq} is the sum of the stress-energy tensor of matter (T_{pq}) and the Landau-Lifshitz pseudotensor for the effective stress-energy of the gravitational field. Since we are using the linearized gravity (appropriate since all gravitational effects are weak; see Ref. [6]), $\tau_{pq} = T_{pq}$. The effective stress-energy tensor for gravity waves is

$$T_{\alpha\beta}^{\text{GW}} = \frac{1}{32\pi G} \sum_{i,j} \langle \partial_\alpha h_{ij}^{TT} \partial_\beta h_{ij}^{TT} \rangle, \quad (42)$$

and the power radiated in terms of the multipoles:

$$P(t) = \frac{G}{32\pi} \sum_{l,m} \left\langle \left| \frac{d^{l+1}}{dt^{l+1}} I^{lm} \right|^2 + \left| \frac{d^{l+1}}{dt^{l+1}} S^{lm} \right|^2 \right\rangle, \quad (43)$$

where $\langle \dots \rangle$ indicates a spatial average over several wavelengths.

The expressions (41) can be simplified considerably. First, only the exponential factor and the Bessel functions depend on ω . The ω integral can be performed explicitly using the identities

$$\int_{-\infty}^{\infty} dx e^{-ixy} j_n(x) = \begin{cases} (-i)^n \pi P_n(y), & |y| < 1; \\ 0, & |y| > 1, \end{cases} \quad (44)$$

where P_n are the Legendre polynomials. This gives

$$\begin{aligned} \frac{d^l}{dt^l} I^{lm}(t) &= 8\pi(-1)^l \int_0^\infty r'^2 dr' \int d\Omega' \int_{-1}^1 d\eta \tau_{pq}(t - \eta r', r', \Omega') \left[a_{-2}(l) T_{pq}^{2l-2, lm}(\Omega')^* P_{l-2}(\eta) \right. \\ &\quad \left. + a_0(l) T_{pq}^{2l, lm}(\Omega')^* P_l(\eta) + a_2(l) T_{pq}^{2l+2, lm}(\Omega')^* P_{l+2}(\eta) \right]. \end{aligned} \quad (45)$$

Now for a single bubble nucleated at $t = 0$, the $O(3, 1)$ symmetry of the scalar-field bubble configuration allows transformation of the radial integral:

$$\begin{aligned} \frac{d^l}{dt^l} I^{lm}(t) &= 8\pi(-1)^l \int_{-1}^1 d\eta \int_0^\infty ds \left(\sqrt{t^2 + s^2(1 - \eta^2)} - t\eta \right)^2 \frac{\sqrt{t^2 + s^2(1 - \eta^2)}}{s(1 - \eta^2)^2} \left(\frac{d\phi}{ds} \right)^2 \\ &\quad \times \left[\sum_{i=-2,0,2} P_i(\eta) \int d\Omega' A^{l+i, lm}(\Omega') \Theta \left(\Omega', \frac{t - \eta \sqrt{t^2 + s^2(1 - \eta^2)}}{1 - \eta^2} \right) \right], \end{aligned} \quad (46)$$

where

$$A^{l, lm}(\Omega') \equiv a_{l-i}(l) T_{pq}^{2l, lm}(\Omega')^* \hat{x}_p(\Omega') \hat{x}_q(\Omega'). \quad (47)$$

Here $s = \sqrt{r^2 - (t - r\eta)^2}$ is the only quantity the scalar field depends upon, $\phi'(s) = \partial\phi/\partial r(r, t = 0)$, and \hat{x} is the unit vector in the direction of Ω' . Explicit expressions for the $A^{l, lm}$ are given in the Appendix. The further substitution

$$y = \frac{t - \eta \sqrt{t^2 + s^2(1 - \eta^2)}}{1 - \eta^2}, \quad \eta = \frac{t - y}{\sqrt{y^2 + s^2}}$$

gives

$$\begin{aligned} \frac{d^l}{dt^l} I^{lm}(t) &= 8\pi(-1)^l \int_0^\infty \frac{ds}{s} \left(\frac{d\phi}{ds} \right)^2 \int_{t/2}^\infty dy \frac{(s^2 + yt)^2}{y^2 + s^2} \\ &\quad \times \left[\sum_{i=-2,0,2} P_{l+i} \left(\frac{t - y}{\sqrt{y^2 + s^2}} \right) \int d\Omega' A^{l+i, lm}(\Omega') \Theta(\Omega', y) \right]. \end{aligned} \quad (48)$$

This expression can be simplified by noting that (1) $d\phi/ds$ is non-zero only when s is smaller than the initial bubble radius, and (2) the angular integral is zero until the bubble first collides, which by assumption is only after the bubble has expanded by a very large factor. Thus $y \gg s$ and to a very good approximation s can be set to zero in the integrand

of the y -integral. Now using Eq. (9b), the s -integral can be performed to give $\rho_{\text{vac}}/3$; Eq. (48) becomes

$$\frac{d^l}{dt^l} I^{lm}(t) = \frac{8\pi}{3} (-1)^l \rho_{\text{vac}} t^2 \int_{t/2}^{\infty} dy \sum_{i=-2,0,2} P_{l+i} \left(\frac{t}{y} - 1 \right) \Theta^{l+i,lm}(y), \quad (49)$$

where

$$\Theta^{l+i,lm}(t) \equiv \int d\Omega' A^{l+i,lm}(\Omega') \Theta(\Omega', t). \quad (50)$$

Note $\Theta^{l+i,lm}$ vanishes (by spherical symmetry) until the bubble first collides; likewise, $\Theta^{l+i,lm}$ vanishes for $t \geq R$, where R is the size of the bubble when its surface has completely collided, since $\Theta(\Omega, t \geq R) = 0$. Analogous formulas hold for the ‘‘current’’ multipole moments S^{lm} , but they vanish because the tensor-spherical harmonics contracted with the unit vectors are identically zero (see Appendix).

The multipole radiation from a single bubble is only nonzero for $0 < t < 2R$. This makes sense physically. The bubble wall propagates outwards at essentially the speed of light; even though the bubble does not begin to radiate until it first collides, the first radiation from the bubble still reaches an observer at distance r at time $t = r$. Likewise, radiation generated on the opposite side of the bubble from the observer will arrive at time $t = r + 2R$, since the diameter of the bubble when it disappears is $2R$.

Equation (49) provides the key to computing the gravitational radiation from a single bubble. The evaluation of $d^l I^{lm}/dt^l$ only involves computing $\Theta^{l+i,lm}(t)$, which depends upon the ‘‘collision history’’ of a given bubble. We present two different estimates for $\Theta^{l+i,lm}(t)$. The first is analytical, based upon the fraction of the bubble surface that remains uncollided at time t ; the second estimate is derived from our numerical simulations of bubble collisions.

Once we have $d^l I^{lm}/dt^l$ in hand for a single bubble, it is a simple matter to calculate the power and the spectrum of the gravitational radiation by summing incoherently over the distribution of bubbles:

$$P(t) = \frac{G}{32\pi} \int_0^{\infty} \sum_{l,m} \left| \frac{d^{l+1}}{dt^{l+1}} I^{lm}(t, R) \right|^2 \frac{dn}{dR} dR; \quad (51)$$

$$\frac{dE_{GW}}{d\omega} = \frac{G\omega^2}{8} \int_0^{\infty} \sum_{l,m} \left| {}^{(l)} I^{lm}(\omega, R) \right|^2 \frac{dn}{dR} dR; \quad (52)$$

where ${}^{(l)} I^{lm}(\omega, R)$ is the Fourier transform of $d^l I^{lm}/dt^l(t, R)$. The R in the argument refers to the multipole radiation from a single bubble whose size at the end of the phase transition is R , and dn/dR is the distribution of bubble sizes, *cf.* Eq. (33). Note that the expressions in Eqs. (51) and (52) are for power and energy per unit volume (since dn/dR is the bubble size distribution per unit volume).

(b) Analytic approximation to $\Theta^{l+i,lm}(t)$

First we consider a very simple analytic approximation. Recall that $\Theta^{l+i,lm}$ is an integral over the uncollided bubble envelope. It must depend upon the fraction of the bubble wall that remains uncollided at time t . This fraction, $f(t, t_R)$, is given by [7]

$$f(t, t_R) = e^{-I(t)+I(t_R)} \quad (53)$$

where t_R is the nucleation time for a bubble which has radius R at the end of the phase transition, *i.e.*, $t_R = t_* - R$. Since $\Theta^{l+i,lm}(t)$ must vanish at early times when the bubble has not yet collided ($f = 1$), and at late times when the bubble surface is completely collided ($f = 0$), $\Theta^{l+i,lm}(t)$ can be expressed as a sum of the terms $(1 - f)^m f^n$ ($n, m = 1, 2, \dots$). We take as a simple *ansatz*

$$\Theta^{l+i,lm}(t) = cf(1 - f) \quad (54)$$

where c is an undetermined normalization constant.

We now estimate gravitational radiation using the quadrupole ($l = 2$) term of the multipole expansion. Taking only the simplest ($i = -2$) term of Eq. (49), we approximate $\ddot{I}^{2m}(t)$ as

$$\frac{d^2}{dt^2} I^{2m}(t, R) = \frac{8\pi}{3} c \rho_{\text{vac}} u^2 \int_{u/2}^{\infty} f(u', R) [1 - f(u', R)] du' \quad (55)$$

where we set $t_* = 0$ as the time origin so that $t_R = -R$, $u = t - t_R = t + R$, and $\Gamma \propto e^{\beta t}$, giving

$$f(u, R) = \exp \left[-M e^{\beta(u-R)} + M e^{-\beta R} \right]; \quad (56)$$

recall $M = I(t_*)$. Note by setting $t_* = 0$ instead of $t_R = 0$, and by using $u = t - t_R$, we take into account that bubbles of different sizes are nucleated at different times. The power radiated in gravitational waves per unit volume is given by the incoherent sum over the distribution of bubble sizes, Eq. (51); we have replaced the sum over m in Eq. (51) with a factor of 5. Likewise, the energy spectrum of gravitational waves per unit volume is given by Eq. (52).

In Fig. 9 we show $P(t)$ and in Fig. 10 we show $\omega dE_{GW}/d\omega$. At low frequencies, the spectrum behaves just as in our many-bubble simulation; however, at high frequencies it falls off more rapidly, and the peak of the spectrum is about a factor of three lower. The deficiency in high frequency power traces to the fact that we have neglected the sharp cusps which form in bubble collisions. In this approximation the fraction of vacuum energy released in gravity waves is $E_{GW}/E_{\text{vac}} = 1.5c^2(H/\beta)^2$, so that $c \simeq 0.2$ reproduces the result of our many-bubble simulations. We have tried a range values for powers of f and $1 - f$ in Eq. (54); these alternatives change only the overall normalization of the spectrum (decreasing with increasing powers).

(c) Numerical estimation of $\Theta^{l+i,lm}(t)$

It is straightforward to extract from our numerical simulations average multipole moments for a single bubble, and thereby determine a normalized approximate spectrum. Specifically, for 70 individual bubbles, nucleated in two of our five smaller simulations, we have computed $d^l I^{lm}(t)/dt^l$ by using Eq. (49), for $l = 2$ and $l = 3$ (the quadrupole and octupole moments). These multipole moments give the gravitational waveforms from a given bubble via Eq. (40); quadrupole and octupole waveforms for a representative bubble are displayed in Fig. 11. The radiated power $P(t)$ for the same bubble is shown in Fig. 12; note that the octupole power is only around 10% of the quadrupole power, so we can safely assume that contributions from higher moments are negligible.

To calculate an “average” energy spectrum from the 70 bubbles, we first construct scaled multipole moments, removing a factor of R from the time variable and a factor of $\rho_{\text{vac}} R^3$ from $d^l I^{lm}(t)/dt^l$ for each bubble. Then we calculate the energy spectrum for each bubble using these scaled moments, and average over the 70 bubbles to give the average spectrum for a bubble. This average energy spectrum, shown in Fig. 13, is quantitatively similar to the two-bubble spectrum, peaking at around $\omega R = 4.6$ with roughly the same overall normalization, but dropping off much faster on the high-frequency side of the peak. We then follow the same procedure as in the previous subsection, integrating over the bubble-size distribution to give the energy spectrum per unit volume of the radiation from the phase transition. The energy per octave is compared with the spectrum from our many-bubble simulation in Fig. 10.

Overall, this statistical approximation does a reasonable job. As with the previous analytical approximations, it closely reproduces the low-frequency behavior. The peak of the approximate spectrum has about the correct amplitude, though the peak frequency is low by about a factor of two. The most obvious discrepancy is again the rapid high-frequency drop of the approximate spectrum, which falls off as ω^{-6} for large frequencies, in marked contrast to the many-bubble calculation, which falls off as $\omega^{-2.8}$. As before, the deficiency of high-frequency power is due to the neglect of cusps. In this approximation the fraction of energy radiated in gravitational waves is $E_{GW}/E_{\text{vac}} = 0.036(H/\beta)^2$, compared with $0.06(H/\beta)^2$ in the many-bubble simulations.

The utility of our pair of statistical approximations lies in their computational ease. The difference in computing time between these approximations and the many-bubble simulations is enormous. In Fig. 10, the analytical statistical approximation required negligible computing time, the numerical statistical approximation used around an hour of computing time, while the many-bubble points required several weeks on the same machine. Furthermore, our averages for the radiation from a single bubble can be used with any form for the bubble nucleation rate, by substituting the appropriate form for dn/dR in Eq. (52). These approximations give a rough, but quick, estimate of the gravitational radiation from any strongly first-order phase transition for which the bubble nucleation rate is known.

V. Discussion and Concluding Remarks

Before summarizing the present work, let us place it in context by reviewing our previous work. Based largely on dimensional estimates, it was argued that the gravitational radiation produced by the collision of vacuum bubbles in a strongly first-order phase transition could account for a substantial fraction of the vacuum energy released [5]. This conjecture was verified in our previous numerical work [6] where we calculated the gravitational radiation resulting from the collision of two vacuum bubbles by evolving the scalar-field configuration corresponding to two vacuum bubbles nucleated simultaneously and separated by distance d . This calculation was carried out in the linearized-gravity approximation and the expansion of the universe was neglected, both assumptions being valid provided that the duration of the transition is less than a Hubble time. We found that the amount of radiation emitted is indeed significant and only depends upon the duration of the collision—and not the fine-scale details of the bubbles. The fraction of vacuum energy liberated into gravitational waves is $E_{\text{GW}}/E_{\text{vac}} \simeq 1.3 \times 10^{-3} (H\tau)^2$, valid for $\tau \sim d$, where τ is the duration of the transition. Unfortunately, this work depended upon the phenomenological parameter τ ; moreover, it is a bold extrapolation to use the collision of two bubbles to model a realistic phase transition, which consists of many bubbles of different sizes colliding. As noted earlier, it is beyond present computational capabilities to collide more than a few bubbles by scalar-field evolution.

These drawbacks led to the present work: the development of a workable approximation to study the gravitational radiation from hundreds of colliding bubbles. Motivated by the fact that our two-bubble results only depend upon the gross features of the collision, we developed the envelope approximation described in this paper. In the envelope approximation an expanding bubble is treated as a very thin shell of energy (equal to the vacuum energy it liberates); when bubbles collide only their envelope is followed and their overlap (interaction) regions are ignored. By considering the collision of two bubbles we showed that the envelope approximation accurately reproduces our previous two-bubble results; *e.g.*, the energy spectrum in gravitational waves agrees to around 20%.

Having established the validity of the envelope approximation, we nucleated hundreds of vacuum bubbles in spherical volumes with a nucleation rate that grows as $e^{\beta t}$: specifically, 127 bubbles total in five small simulations and 180 bubbles in one large simulation. (It is argued in Ref. [7] that such a functional dependence for the bubble-nucleation rate applies with great generality.) Using the envelope approximation we computed the fraction of vacuum energy released in gravitational waves and found: $E_{\text{GW}}/E_{\text{vac}} \simeq 0.06 (H/\beta)^2$ with the energy spectrum peaking at a frequency $\omega \simeq 1.6\beta (H^2 = 8\pi G\rho_{\text{vac}}/3)$. With this nucleation rate the duration of the phase transition $\tau \simeq 3/\beta$; using this fact, it follows that the fraction of energy liberated in gravitational waves is about five times the estimate based upon our previous two-bubble results, with the spectrum peaking at about the same frequency. We believe that additional energy is released in gravity waves because a given

bubble collides with many other bubbles rather than a single bubble.

In the present work we also have developed two statistical approximations that allow simple analytical or semi-analytical approximations to the energy spectrum radiated in gravitational waves. Both approximations provide better than order-of-magnitude accuracy and greater ease of calculation, and are particularly well suited to computing the gravitational radiation for an arbitrary bubble nucleation rate.

On very general grounds it has been argued that β^{-1} , which controls the time/length scale of the phase transition, is of the order of a few percent of H^{-1} or greater (see Section IV or Ref. [7]), indicating that the fraction of vacuum energy liberated in gravitational waves in a phase transition that proceeds through the nucleation and collision of vacuum bubbles is of order 10^{-4} or so. We have addressed the potential observational consequences of our results in a *Letter* [8]; very briefly, in terms of the temperature of the universe after the phase transition, the fraction of critical density contributed by gravitational waves produced is $\Omega_{\text{GW}} \sim 10^{-9}$ with characteristic frequency $f \sim 10^{-6} (T/\text{GeV}) \text{ Hz}$. There we also discuss the prospects for the detection of such a stochastic background of gravitational waves with the coming generation of laser interferometer gravity-wave observatories [14].

Two key assumptions underlay all of our work: (1) the use of linearized gravity and the neglect of the expansion of the universe; and (2) the assumption that the bubbles expand at constant acceleration (put another way, all the vacuum energy liberated is converted into the kinetic energy of the bubble wall). As we discussed in Ref. [6] the first assumption is valid so long as the duration of the phase transition $\tau \sim \beta^{-1}$ is much less than the Hubble time H^{-1} . This should be satisfied for most phase transitions as β^{-1} is expected to be only a few percent of H^{-1} . However, there are situations where this condition may not be satisfied, *e.g.*, in some models of extended inflation [15]; moreover, such situations are very interesting since our results indicate that the fraction of energy liberated in gravity waves approaches unity. We are currently trying to generalize our results by relaxing the first assumption [16].

The second assumption is that all the vacuum energy liberated by a bubble goes into the kinetic energy of its wall. This is certainly true for a bubble nucleated at zero temperature, but it may not be a good approximation to one nucleated at finite temperature because of the interaction of the bubble with the ambient thermal plasma. The second assumption is certainly well justified for models of first-order inflation where the universe has undergone extreme supercooling during the inflationary epoch so that the temperature of the Universe when the phase transition occurs is exponentially small. Whether or not this assumption applies in a first-order phase transition that only undergoes moderate supercooling is an open question. In this case it is not implausible that much or even most of the latent heat released is dissipated into heat rather than the bulk motion of the expanding bubble front (here we have used the term latent heat rather than vacuum energy). The motion of a bubble wall in this circumstance is not a simple matter to analyze: both the microscopic interaction of the ambient medium with the bubble front and bulk hydrodynamics are

important. Though much work has been done the results are not conclusive [17].

The strength of a first-order phase transition can be characterized by the ratio of the latent heat (per unit volume) released to the energy density of the ambient plasma, given by the fourth power of the temperature at which bubble nucleation commences: $\gamma = \rho_{\text{vac}}/T_{\text{nuc}}^4$; note that the increase in entropy per comoving is proportional to $\gamma^{3/4}$. For an inflationary transition $\gamma \rightarrow \infty$, while for a weakly first-order transition γ is of order unity or less. For very large γ it seems clear that the bubbles must behave as vacuum bubbles (all the latent heat liberated goes into accelerating the bubble wall). What happens for moderate values of γ is still unclear and probably depends on the specific phase transition under consideration. The latent heat could simply be dissipated viscously, in which case little gravitational radiation would be produced; or the latent heat could be converted into the bulk motion of the fluid (at some velocity less than the speed of light), in which case an appreciable amount of gravitational radiation could still be produced. This important issue is currently under study [18].

Acknowledgements

We thank Erick Weinberg, Rick Davis, John Preskill, and Paul Steinhardt for helpful discussions. This work has been supported by a National Science Foundation graduate fellowship, the NASA Graduate Student Researchers Program, by the DOE (at Chicago and Fermilab), and by NASA through grant NAGW-2381 (at Fermilab).

Appendix: Tensor Spherical Harmonics

In this appendix we review the formalism of tensor-spherical harmonics, and calculate the tensor contractions needed in Sec. IV. Generally, we follow the notation presented in [13]. A set of basis vectors ξ^m are coupled to form the traceless and symmetric basis tensors \mathbf{t}^m :

$$\mathbf{t}^m = \sum_{m'=-1}^{+1} \sum_{m''=-1}^{+1} (1\ 1\ m'\ m''|2\ m) \xi^{m'} \otimes \xi^{m''} \quad (\text{A.1a})$$

where $(l_1\ l_2\ m_1\ m_2|l_3\ m_3)$ is the Clebsch-Gordan coefficient for adding angular momenta l_1 and l_2 to obtain l_3 . In terms of the Cartesian basis vectors \mathbf{e}_x , \mathbf{e}_y , and \mathbf{e}_z , these symmetric basis tensors are

$$\mathbf{t}^{\pm 2} = \frac{1}{2}(\mathbf{e}_x \otimes \mathbf{e}_x - \mathbf{e}_y \otimes \mathbf{e}_y) \pm \frac{i}{2}(\mathbf{e}_x \otimes \mathbf{e}_y + \mathbf{e}_y \otimes \mathbf{e}_x); \quad (\text{A.1b})$$

$$\mathbf{t}^{\pm 1} = \mp \frac{1}{2}(\mathbf{e}_x \otimes \mathbf{e}_z + \mathbf{e}_z \otimes \mathbf{e}_x) - \frac{i}{2}(\mathbf{e}_y \otimes \mathbf{e}_z + \mathbf{e}_z \otimes \mathbf{e}_y); \quad (\text{A.1c})$$

$$\mathbf{t}^0 = \frac{1}{\sqrt{6}}(2\mathbf{e}_z \otimes \mathbf{e}_z - \mathbf{e}_x \otimes \mathbf{e}_x - \mathbf{e}_y \otimes \mathbf{e}_y). \quad (\text{A.1d})$$

Then the relevant tensor spherical harmonics are

$$\mathbb{T}^{2l',lm} = \sum_{m'=-l'}^{l'} \sum_{m''=-2}^2 (l' 2 m' m'' | l m) Y^{l' m'} t^{m''}, \quad (\text{A.2})$$

where $l' = l, l \pm 1, l \pm 2$. This represents the combination of an orbital angular momentum l' and a spin angular momentum 2 to give total angular momentum l . These spherical harmonics are eigenfunctions of the orbital angular momentum operator \mathbf{L}^2 with eigenvalue $l(l+1)$, like the more familiar Y^{lm} . Also, we have the “pure spin tensor harmonics” for spin 2,

$$\mathbb{T}^{E2,lm} = a_2(l)\mathbb{T}^{2l+2,lm} + a_0(l)\mathbb{T}^{2l,lm} + a_{-2}(l)\mathbb{T}^{2l-2,lm}; \quad (\text{A.3a})$$

$$\mathbb{T}^{B2,lm} = -ia_1(l)\mathbb{T}^{2l+1,lm} - ia_{-1}(l)\mathbb{T}^{2l-1,lm}; \quad (\text{A.3b})$$

where

$$a_2(l) \equiv \sqrt{\frac{l(l-1)}{2(2l+1)(2l+3)}}; \quad (\text{A.4a})$$

$$a_1(l) \equiv \sqrt{\frac{l-1}{2l+1}}; \quad (\text{A.4b})$$

$$a_0(l) \equiv \sqrt{\frac{3(l-1)(l+2)}{(2l-1)(2l+3)}}; \quad (\text{A.4c})$$

$$a_{-1}(l) \equiv \sqrt{\frac{l+2}{2l+1}}; \quad (\text{A.4d})$$

$$a_{-2}(l) \equiv \sqrt{\frac{(l+1)(l+2)}{2(2l+1)(2l-1)}}. \quad (\text{A.4e})$$

Under rotations around the radial vector, the harmonics (A.3) transform like the components of the polarization tensor of a pure spin-2 state, but they are not orbital angular momentum eigenfunctions.

Using the above definitions, it is straightforward to calculate the explicit forms for the necessary tensor contractions. Equation (47) defines the auxiliary quantity

$$A^{l',lm}(\Omega) \equiv a_{l'-l}(l)\mathbb{T}_{pq}^{2l',lm}(\Omega) \hat{x}_p(\Omega)\hat{x}_q(\Omega)$$

where \hat{x} is a unit vector in the direction Ω . The expressions for $m < 0$ follow from the identity

$$\mathbb{T}^{2l',lm} = (-1)^{l'+l+m}(\mathbb{T}^{2l',l-m})^* \quad (\text{A.5})$$

For $l = 2$ (quadrupole moments):

$$A^{l',2m} = 0 \quad \text{for} \quad l' = 1, \quad l' = 3 \quad (\text{A.6})$$

$$A^{0,22} = \frac{1}{4} \sqrt{\frac{2}{5\pi}} e^{-2i\phi} \sin^2 \theta \quad (\text{A.7})$$

$$A^{2,22} = -\frac{5}{28} \sqrt{\frac{2}{5\pi}} e^{-2i\phi} (1 + \sin^2 \theta + 2 \sin^4 \theta) \quad (\text{A.8})$$

$$A^{4,22} = \frac{3}{28} \sqrt{\frac{2}{5\pi}} e^{-2i\phi} \sin^2 \theta \quad (\text{A.9})$$

$$A^{0,21} = -\frac{1}{4} \sqrt{\frac{2}{5\pi}} e^{-i\phi} \sin 2\theta \quad (\text{A.10})$$

$$A^{2,21} = \frac{5}{112} \sqrt{\frac{2}{5\pi}} e^{-i\phi} (8 - 2 \cos 2\theta - \sin 4\theta) \quad (\text{A.11})$$

$$A^{4,21} = -\frac{3}{28} \sqrt{\frac{2}{5\pi}} e^{-i\phi} \sin 2\theta \quad (\text{A.12})$$

$$A^{0,20} = -\frac{1}{6} \sqrt{\frac{3}{5\pi}} (1 - 3 \cos^2 \theta) \quad (\text{A.13})$$

$$A^{2,20} = -\frac{5}{42} \sqrt{\frac{3}{5\pi}} (1 + 3 \cos 2\theta) \quad (\text{A.14})$$

$$A^{4,20} = \frac{1}{28} \sqrt{\frac{3}{5\pi}} (1 + 3 \cos 2\theta) \quad (\text{A.15})$$

For $l = 3$ (octupole moments):

$$A^{l',3m} = 0 \quad \text{for} \quad l' = 2, \quad l' = 4 \quad (\text{A.16})$$

$$A^{1,33} = -\frac{1}{4} \sqrt{\frac{3}{7\pi}} e^{-3i\phi} \sin^3 \theta \quad (\text{A.17})$$

$$A^{3,33} = \frac{7}{18} \sqrt{\frac{3}{7\pi}} e^{-3i\phi} \sin^3 \theta \quad (\text{A.18})$$

$$A^{5,33} = -\frac{5}{36} \sqrt{\frac{3}{7\pi}} e^{-3i\phi} \sin^3 \theta \quad (\text{A.19})$$

$$A^{1,32} = \frac{3}{4} \sqrt{\frac{2}{7\pi}} e^{-2i\phi} \cos \theta \sin^2 \theta \quad (\text{A.20})$$

$$A^{3,32} = -\frac{7}{6} \sqrt{\frac{2}{7\pi}} e^{-2i\phi} \cos \theta \sin^2 \theta \quad (\text{A.21})$$

$$A^{5,32} = \frac{5}{12} \sqrt{\frac{2}{7\pi}} e^{-2i\phi} \cos \theta \sin^2 \theta \quad (\text{A.22})$$

$$A^{1,31} = -\sqrt{\frac{5}{7\pi}} e^{-i\phi} \sin \theta \left[\frac{9}{40} + \frac{3}{8} \cos 2\theta \right] \quad (\text{A.23})$$

$$A^{3,31} = -\sqrt{\frac{5}{7\pi}} e^{-i\phi} \sin \theta \left[\frac{21}{80} + \frac{7}{12} \cos 2\theta - \frac{7}{96} \cos 4\theta \right] \quad (\text{A.24})$$

$$A^{5,31} = -\sqrt{\frac{5}{7\pi}} e^{-i\phi} \sin \theta \left[\frac{1}{8} + \frac{5}{24} \cos 2\theta \right] \quad (\text{A.25})$$

$$A^{1,30} = \sqrt{\frac{5}{21\pi}} \cos \theta \left[\frac{3}{4} \cos 2\theta - \frac{3}{20} \right] \quad (\text{A.26})$$

$$A^{3,30} = -\sqrt{\frac{5}{21\pi}} \left[\frac{7}{20} \cos \theta + \frac{7}{12} \cos 3\theta \right] \quad (\text{A.27})$$

$$A^{5,30} = \sqrt{\frac{5}{21\pi}} \left[\frac{1}{8} \cos \theta + \frac{5}{24} \cos 3\theta \right] \quad (\text{A.28})$$

References

- [1] V. A. Rubakov, M. Sazhin, and A. Veryaskin, *Phys. Lett.* **115B**, 189 (1982); R. Fabbri and M. Pollack, *ibid.* **125B**, 445 (1983).
- [2] T. Vachaspati and A. Vilenkin, *Phys. Rev. D* **31**, 3052 (1985); T. Vachaspati, A. E. Everett, and A. Vilenkin, *ibid.* **30**, 2046 (1984); B. Allen and E. P. S. Shellard, *ibid.* **45**, 1898 (1992); R. R. Caldwell and B. Allen, *ibid.* **45**, 3447 (1992).
- [3] B. J. Carr, *Astron. and Astrophys.* **89**, 6 (1980).
- [4] C. J. Hogan, *Mon. Not. R. Astron. Soc.* **218**, 629 (1986); E. Witten, *Phys. Rev. D* **30**, 272 (1984); L. M. Krauss, *Phys. Lett.* **B284**, 229 (1992).
- [5] M. S. Turner and F. Wilczek, *Phys. Rev. Lett.* **65**, 3080 (1990).
- [6] A. Kosowsky, M. S. Turner, and R. Watkins, *Phys. Rev. D* **45**, 4514 (1992).
- [7] M. S. Turner, E. J. Weinberg, and L. M. Widrow, *Phys. Rev. D* **46**, 2384 (1992).
- [8] A. Kosowsky, M.S. Turner, and R. Watkins, *Phys. Rev. Lett.* **69**, 2026 (1992).
- [9] S. Coleman, *Phys. Rev. D* **15**, 2929 (1977); C. Callan and S. Coleman, *ibid.* **16**, 1762 (1977).
- [10] For a detailed discussion of vacuum bubble kinematics, see S. W. Hawking, J. M. Stewart, and I. G. Moss, *Phys. Rev. D* **26**, 2681 (1982); also, R. Watkins and L. Widrow, *Nuc. Phys. B* **374**, 446 (1992).
- [11] S. Weinberg, *Gravitation and Cosmology* (Wiley, New York, 1972), Ch. 10.
- [12] A. H. Guth and H. Tye, *Phys. Rev. Lett.* **44**, 631 (1980); *ibid.* **44**, 963(E) (1980).
- [13] K. S. Thorne, *Rev. Mod. Phys.* **52**, 299 (1980).
- [14] A. Abramovici *et al.*, *Science* **256**, 325 (1992); J. E. Faller *et al.*, *Adv. Space Res.* **9**, 107 (1989).

- [15] For a discussion of extended inflation, see D. La and P. J. Steinhardt, *Phys. Rev. Lett.* **62**, 376 (1989); E. J. Weinberg, *Phys. Rev. D* **40**, 3950 (1989); and E. W. Kolb, *Phys. Scr.* **T36**, 199 (1991).
- [16] A. Kosowsky, M.S. Turner, and E. Weinberg, unpublished.
- [17] D. A. Kirzhnits, *JETP Lett.* **15**, 529 (1972); D. A. Kirzhnits and A. D. Linde, *Ann. Phys.* **101**, 195 (1976); M. Dine *et al.*, *Phys. Rev. D* **46**, 550 (1992); M. Gyulassy *et al.*, *Nuc. Phys B* **237**, 477 (1984); K. Enqvist *et al.*, *Phys. Rev. D* **45**, 3415 (1992); M. Kamionkowski and K. Freese, Institute for Advanced Studies Report No. IASSNS-HEP-92/46 (1992), unpublished; P. J. Steinhardt, *Phys. Rev. D* **25**, 2082 (1982); B. Liu, L. McLerran, and N. Turok, *Phys. Rev. D* **46**, 2668 (1992).
- [18] M. Kamionkowski, A. Kosowsky, and M.S. Turner, unpublished.

Figure Captions

Figure 1: The kinetic (dashed curve), gradient (dot-dashed curve), and total (solid curve) energy of a single expanding vacuum bubble. The scales are arbitrary; the bubble has initial radius of about 10, in the same units as t . Note that by $t = 20$, when the bubble has approximately doubled in size, the total energy scales almost exactly as t^3 , the vacuum energy liberated by a bubble expanding at the speed of light from zero initial size, and resides equally in the kinetic and gradient energies of the bubble wall.

Figure 2: A schematic picture that illustrates the envelope approximation. The dark lines are the bubble walls, expanding at the speed of light. The shaded areas are the interaction regions; the envelope approximation neglects the interaction regions and takes into account only the bubble envelopes. Snapshot (b) is at a somewhat later time, and three new bubbles have been nucleated.

Figure 3: The energy spectrum of radiation from two colliding bubbles, in the quadrupole approximation. The units are the same for both curves, but arbitrary. The dashed curve is the result from detailed scalar field evolution (Ref. [6]), and the solid curve from the envelope approximation.

Figure 4: The energy spectrum from two colliding bubbles in the full linearized-gravity approximation. The units are the same as in Fig. 3. The solid line is the envelope approximation, which reproduces well the results from detailed scalar-field evolution [6], the dashed curve.

Figure 5: The distribution of bubble sizes, both unweighted and weighted by the bubble's total energy, for the exponential nucleation rate $\Gamma(t) = \Gamma_0 e^{\beta t}$. The energy-weighted distribution peaks at a radius that is almost twice as large.

Figure 6: A slice through a spherical sample volume at different times. The volume boundary is the outer circle; the bubble walls are the darker curves within the boundary. A total of 33 bubbles were nucleated in this volume during the phase transition.

Figure 7: The differential energy spectrum $dE/d\omega d\Omega$, for three orthogonal directions in a simulation with 33 colliding bubbles. Note the large variations in the different directions.

Figure 8: The energy spectrum per frequency octave, divided by the vacuum energy of the sample volume. The points with error flags are averaged over the five different simulations and integrated over six directions per simulation. The error bars reflect the standard estimate for the deviation of the mean. The dashed line is the spectrum for two bubbles, calculated using scalar-field evolution [6], with $\tau = 3.2\beta$. The solid triangles are the results of the 180-bubble simulation (integrated over six directions).

Figure 9: The radiated power $P(t)$ per unit volume in the first statistical approximation. The phase transition completes at $t = 0$.

Figure 10: The energy spectrum as computed in the first statistical approximation, with $c = 1$ (solid line) and the spectrum from the second statistical approximation (dashed line), compared with the results of our many-bubble simulations (points with error flags).

Figure 11: The quadrupole and octupole moments for a given bubble nucleated at time zero. R is the final bubble radius. (a) The real and imaginary parts of the quadrupole moments for $m = 0, 1, 2$ (the imaginary part of the $m = 0$ moments vanish). (b) The same for the octupole moments for $m = 0, 1, 2, 3$.

Figure 12: The quadrupole (upper curve) and octupole (lower curve) contributions to the total power radiated from the bubble in Fig. 10.

Figure 13: The mean energy spectrum of a “typical” bubble, derived by averaging over 70 individual bubbles. The standard estimate for the deviation of the mean is around $\pm 10\%$.

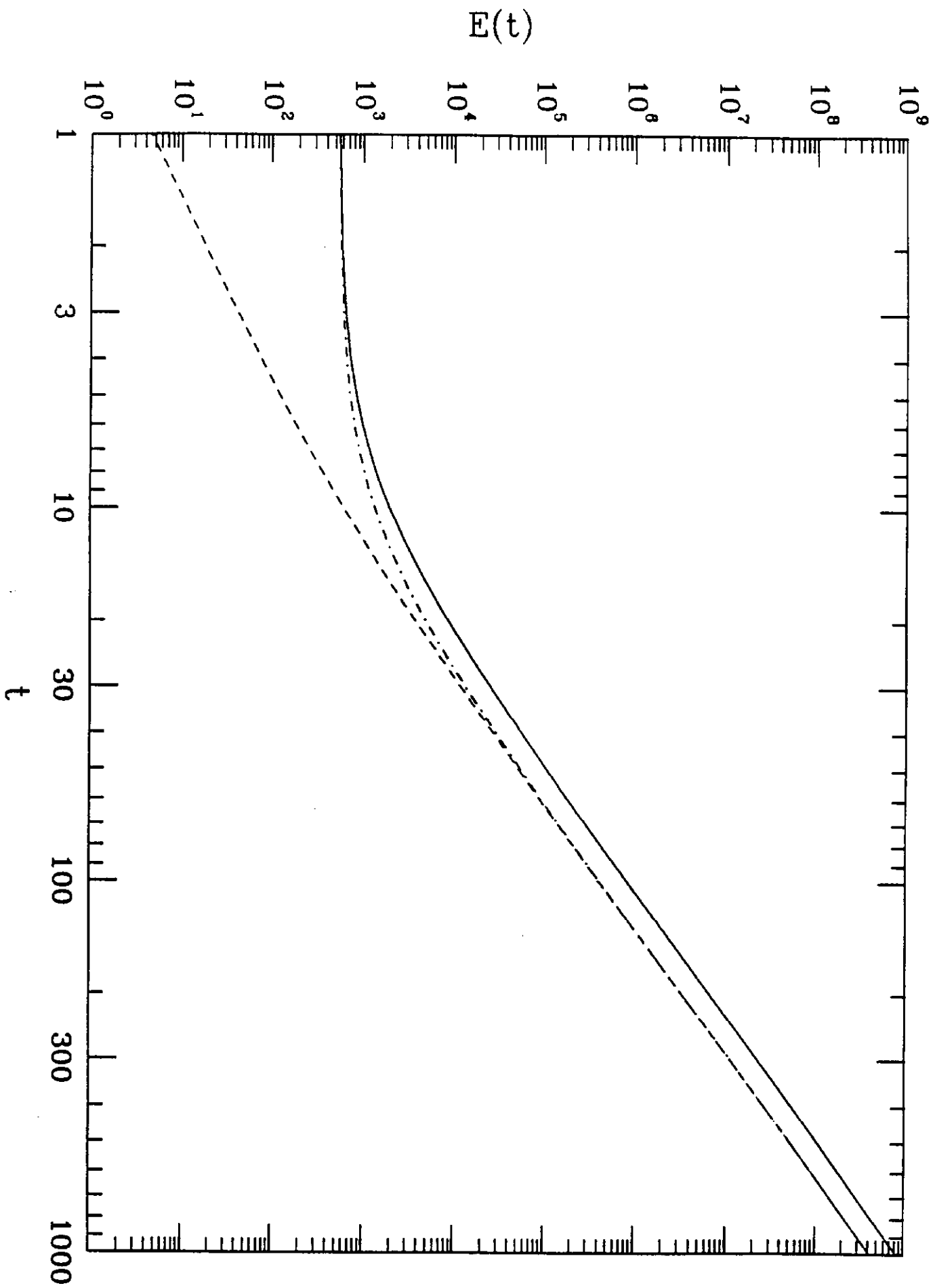


Figure 1

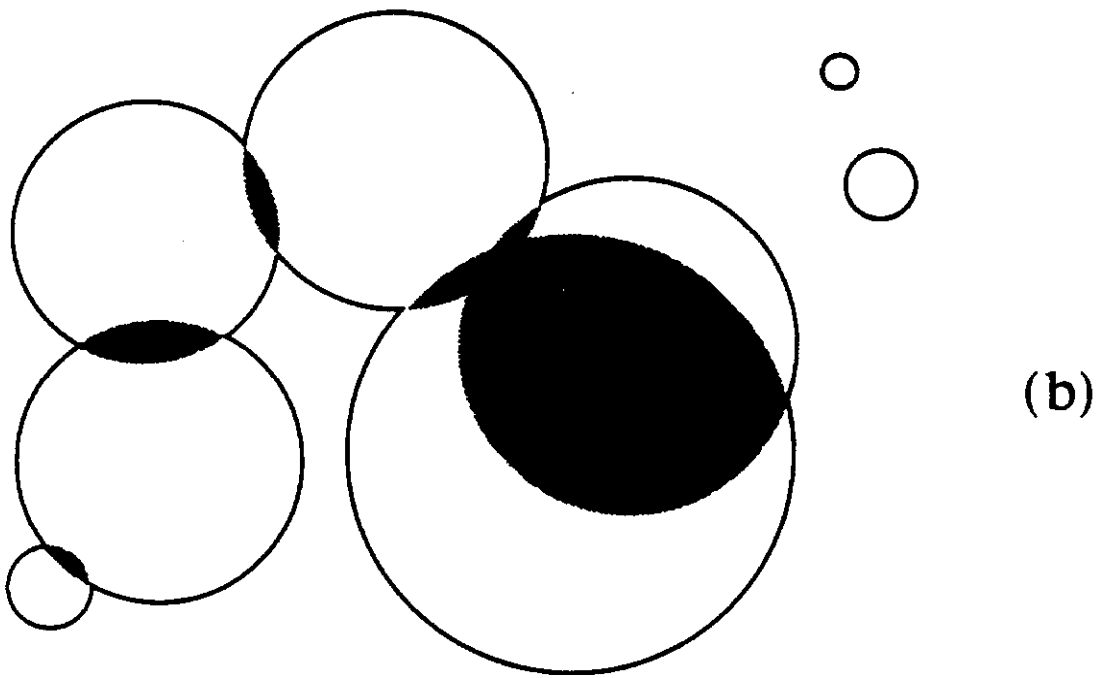
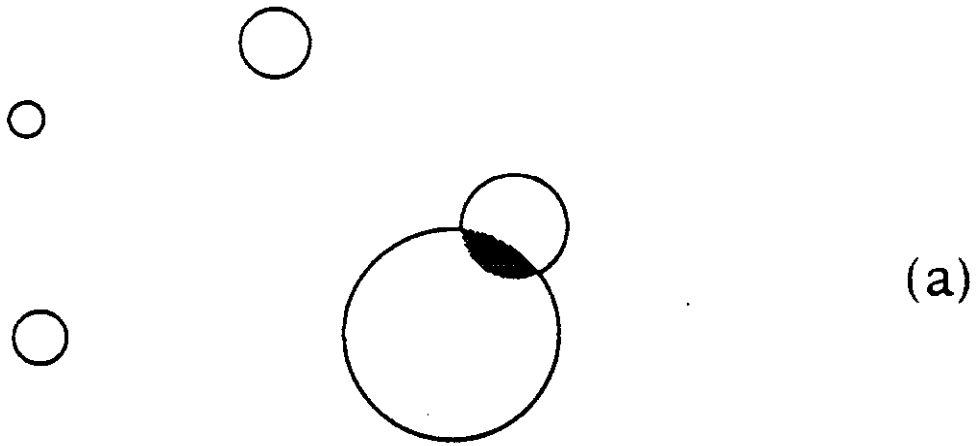


Figure 2

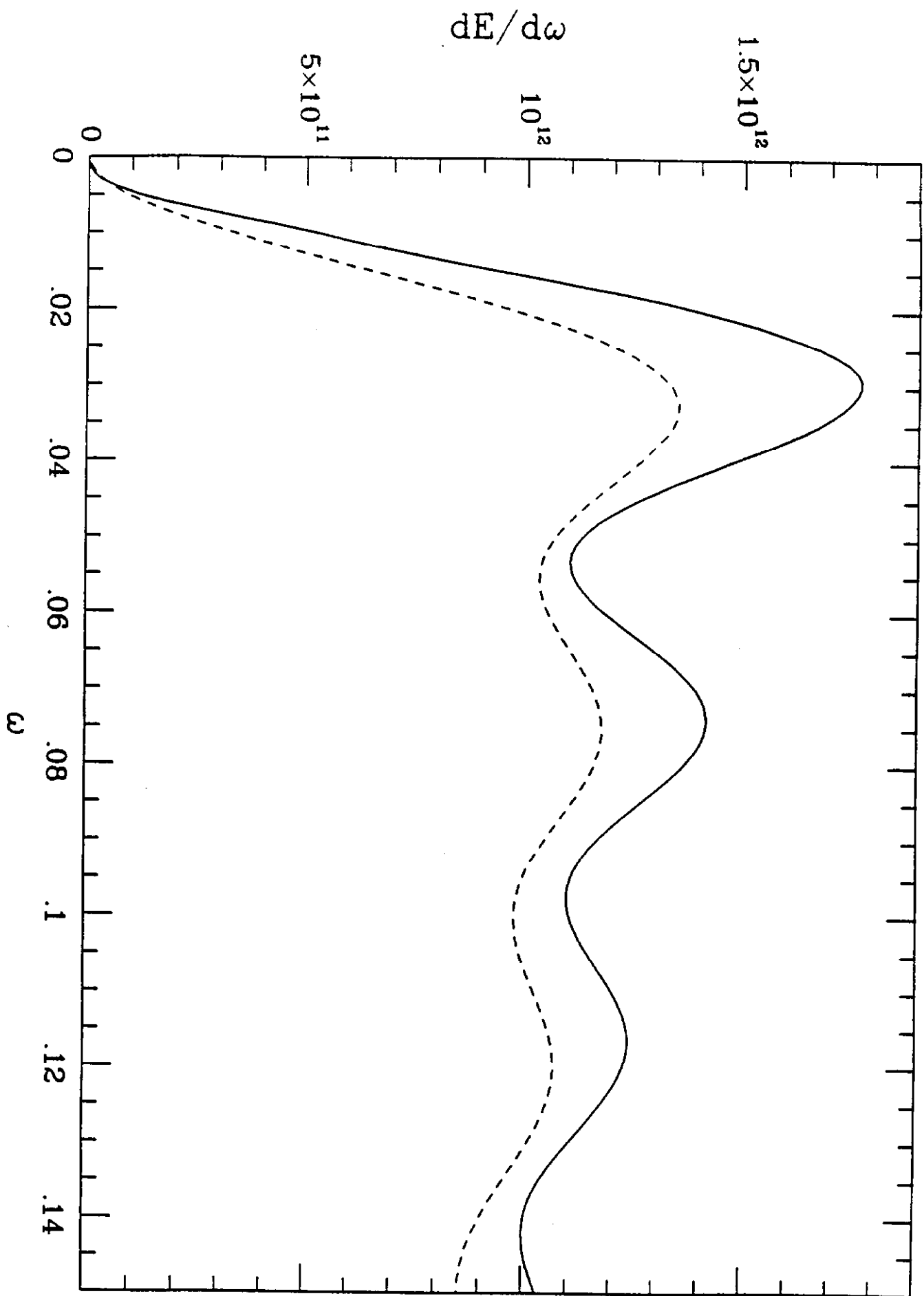


Figure 3

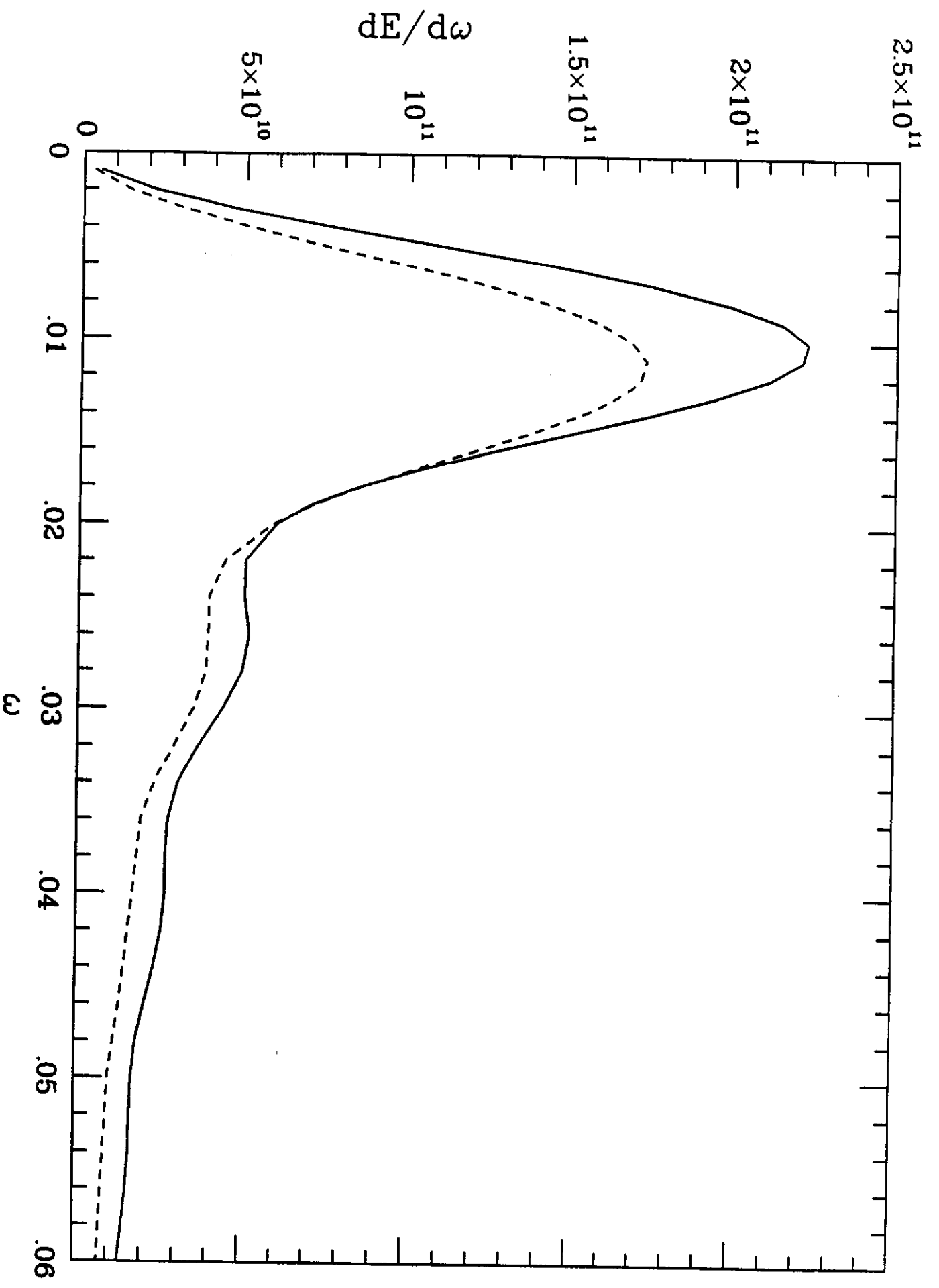


Figure 4

$(dn/dr)/\beta^4, (dn_E/dr)/100\beta\rho_{vac}$

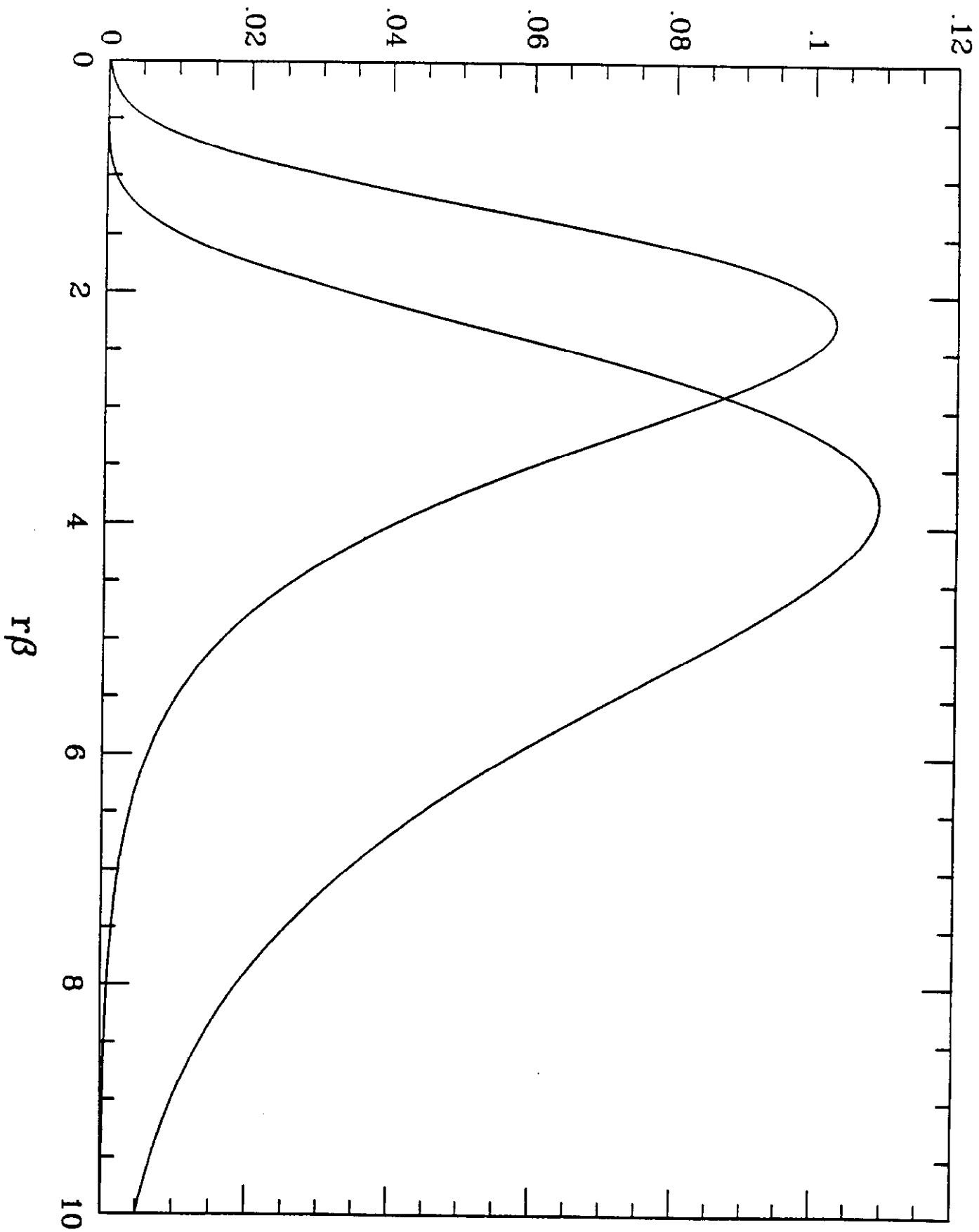
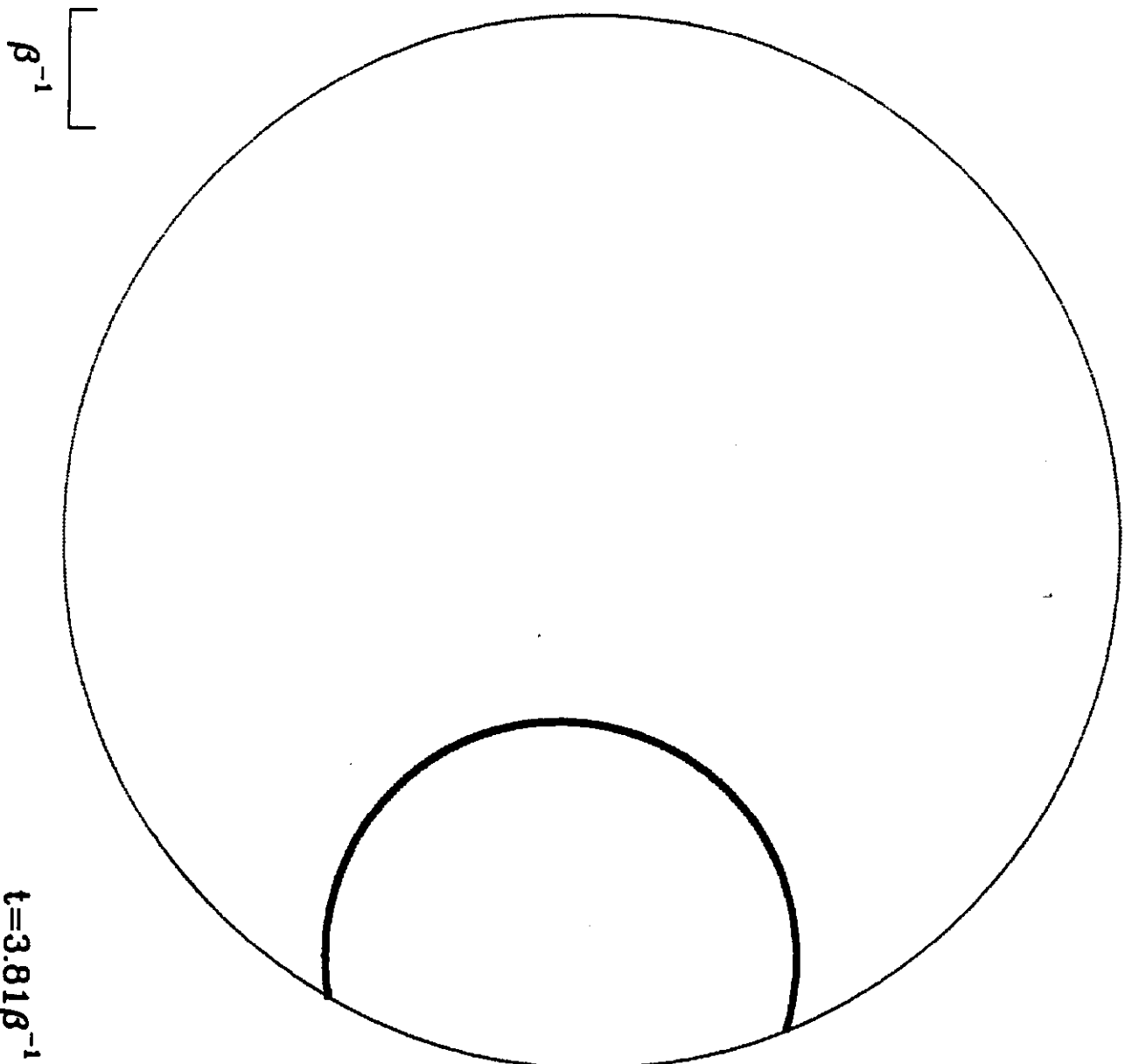
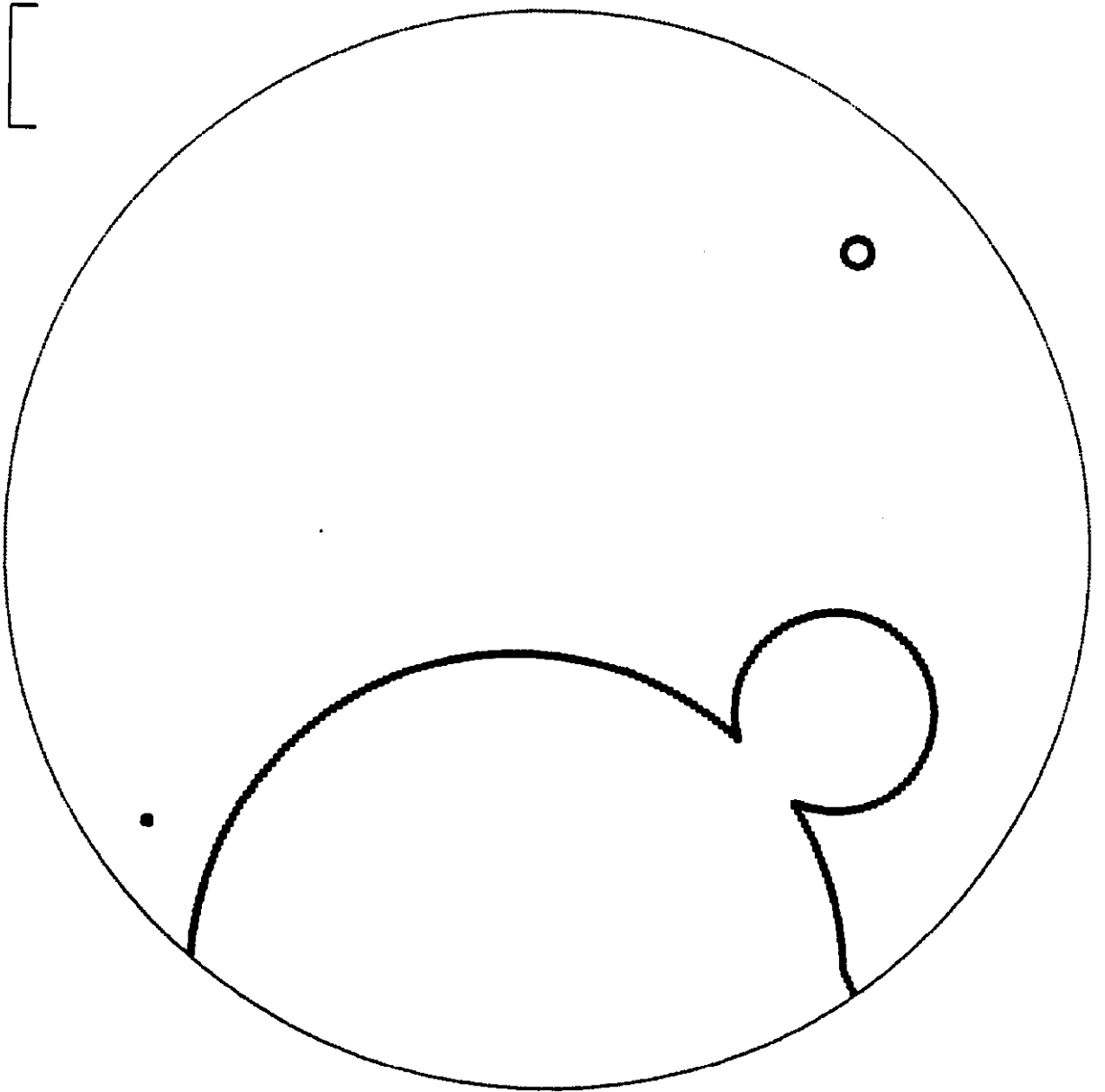


Figure 5



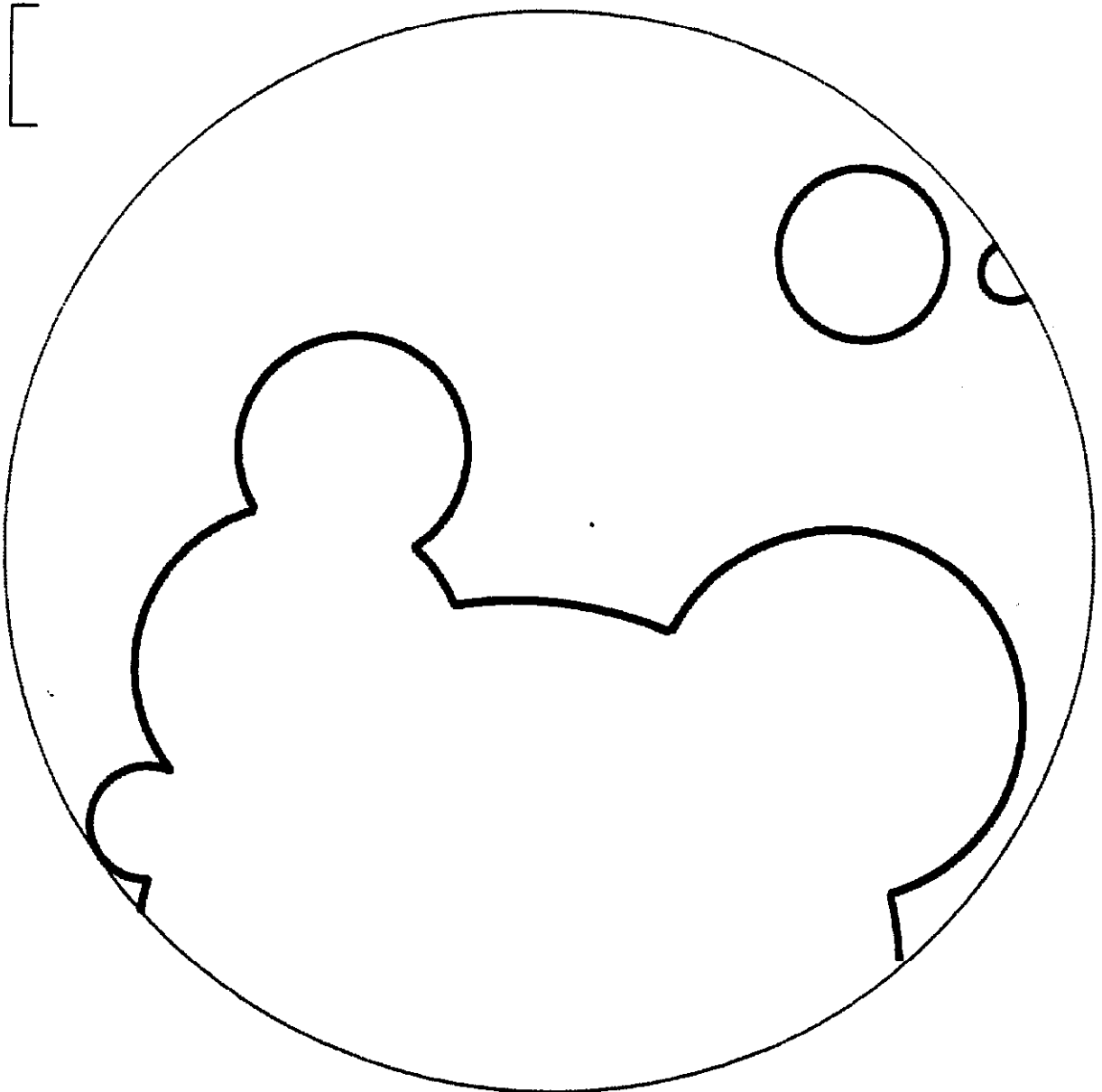
(a)



β^{-1}

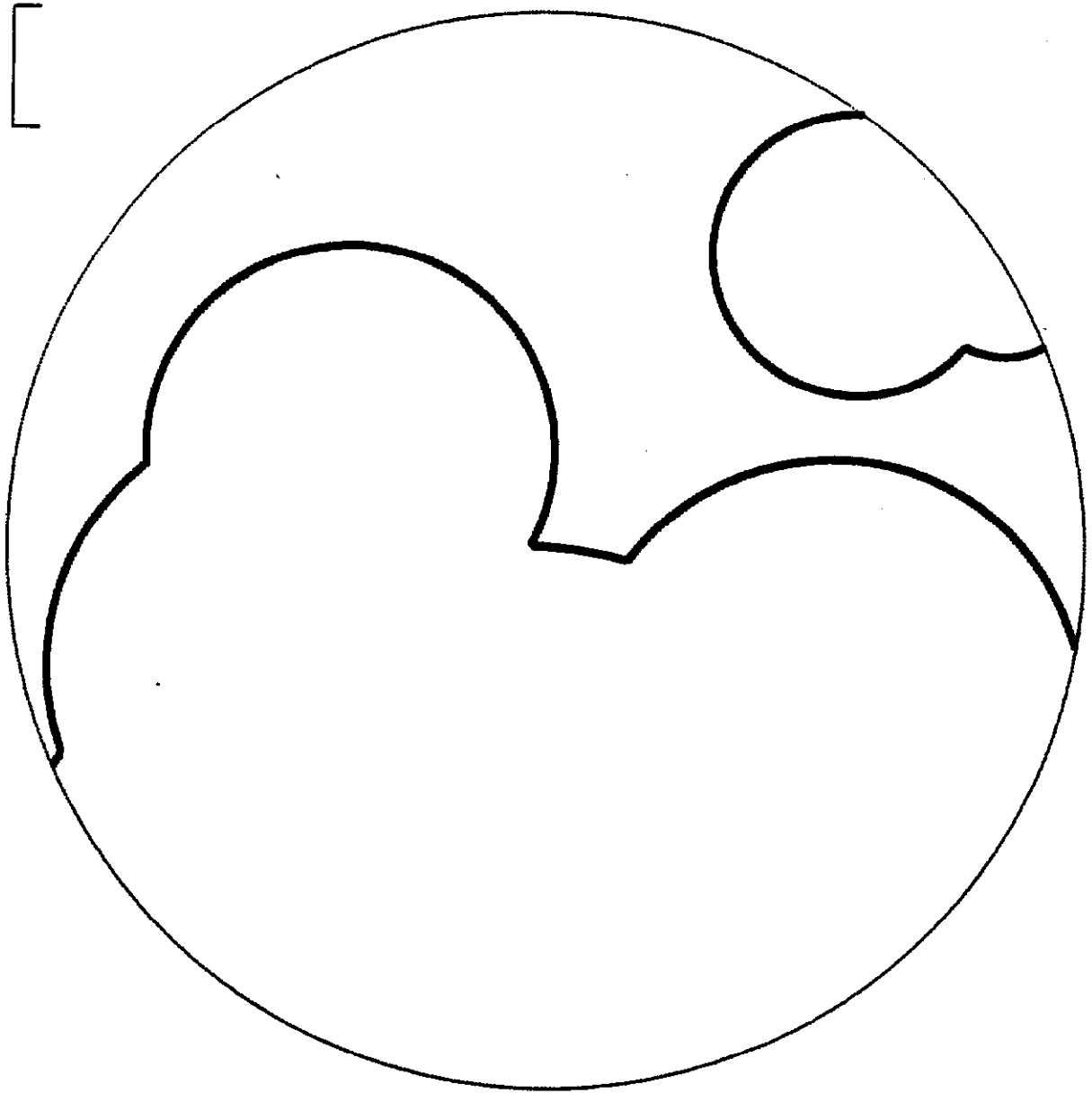
$t=4.48\beta^{-1}$

(b)



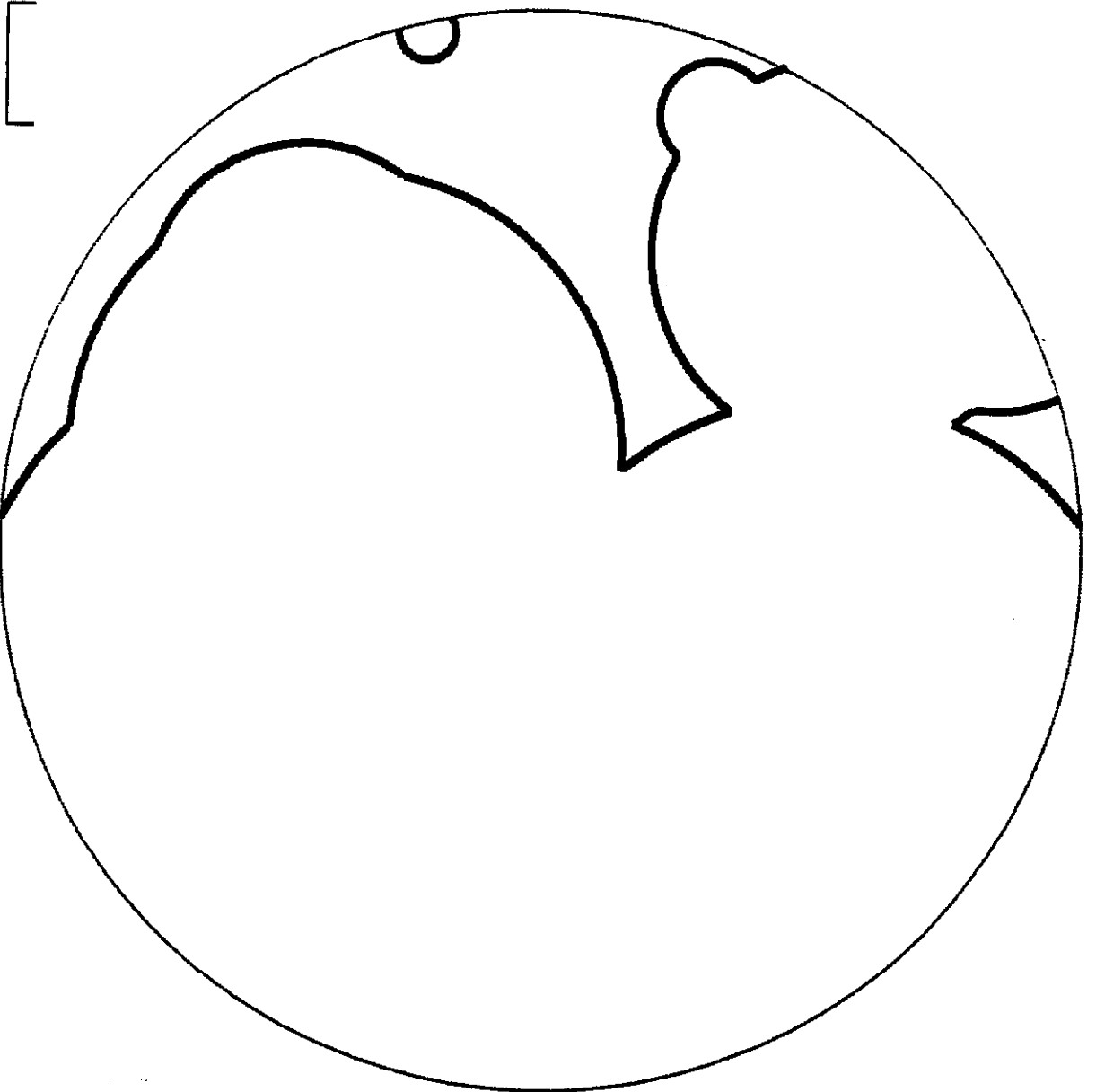
(c)

$t=4.93\beta^{-1}$



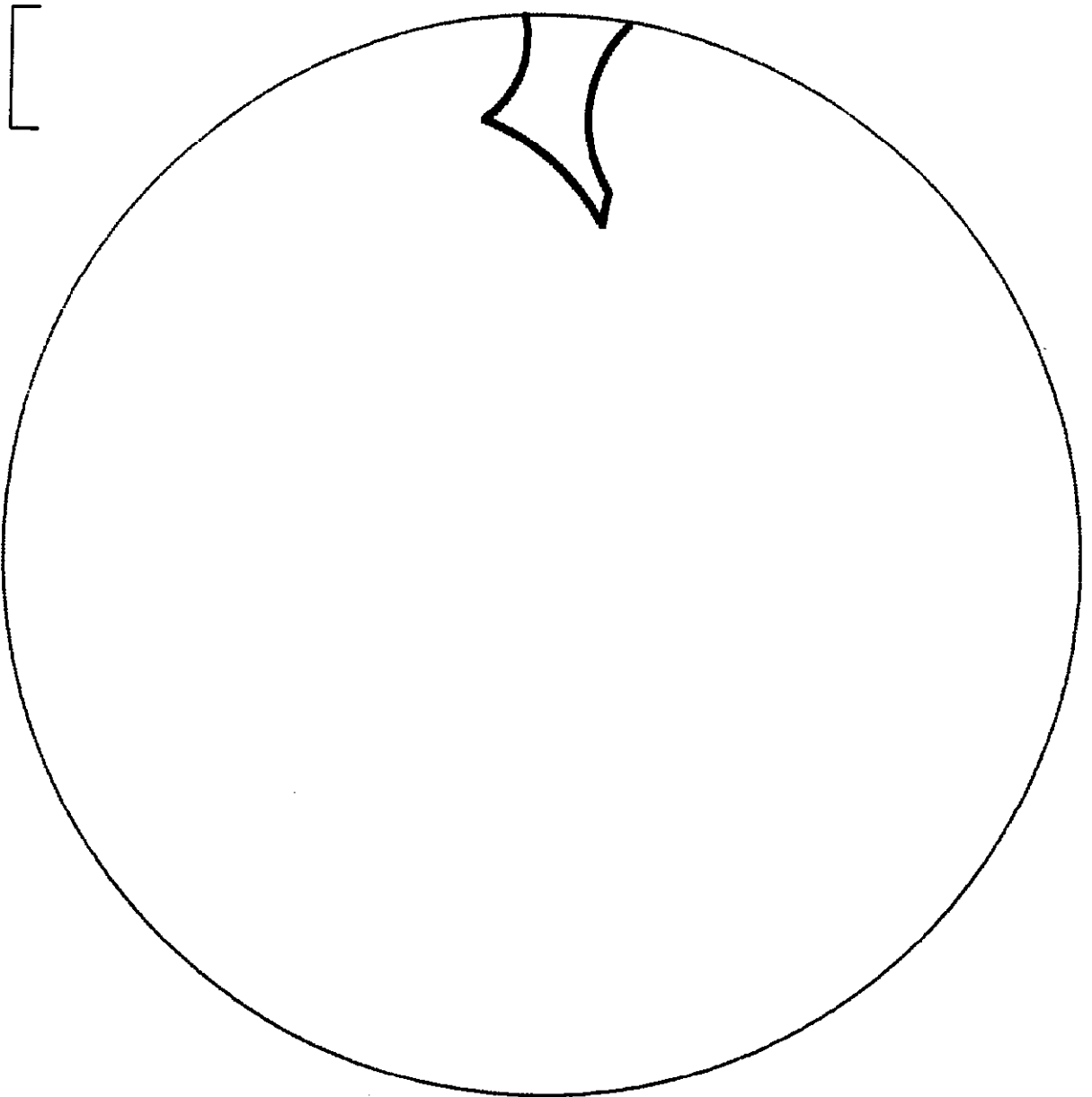
$t=5.38\beta^{-1}$

(d)



$t=5.83\beta^{-1}$

(e)



β^{-1}

(f)

$t=6.28\beta^{-1}$

$$dE/d\omega d\Omega \text{ (} G\rho_{\text{vac}}^2/\beta^6 \text{)}$$

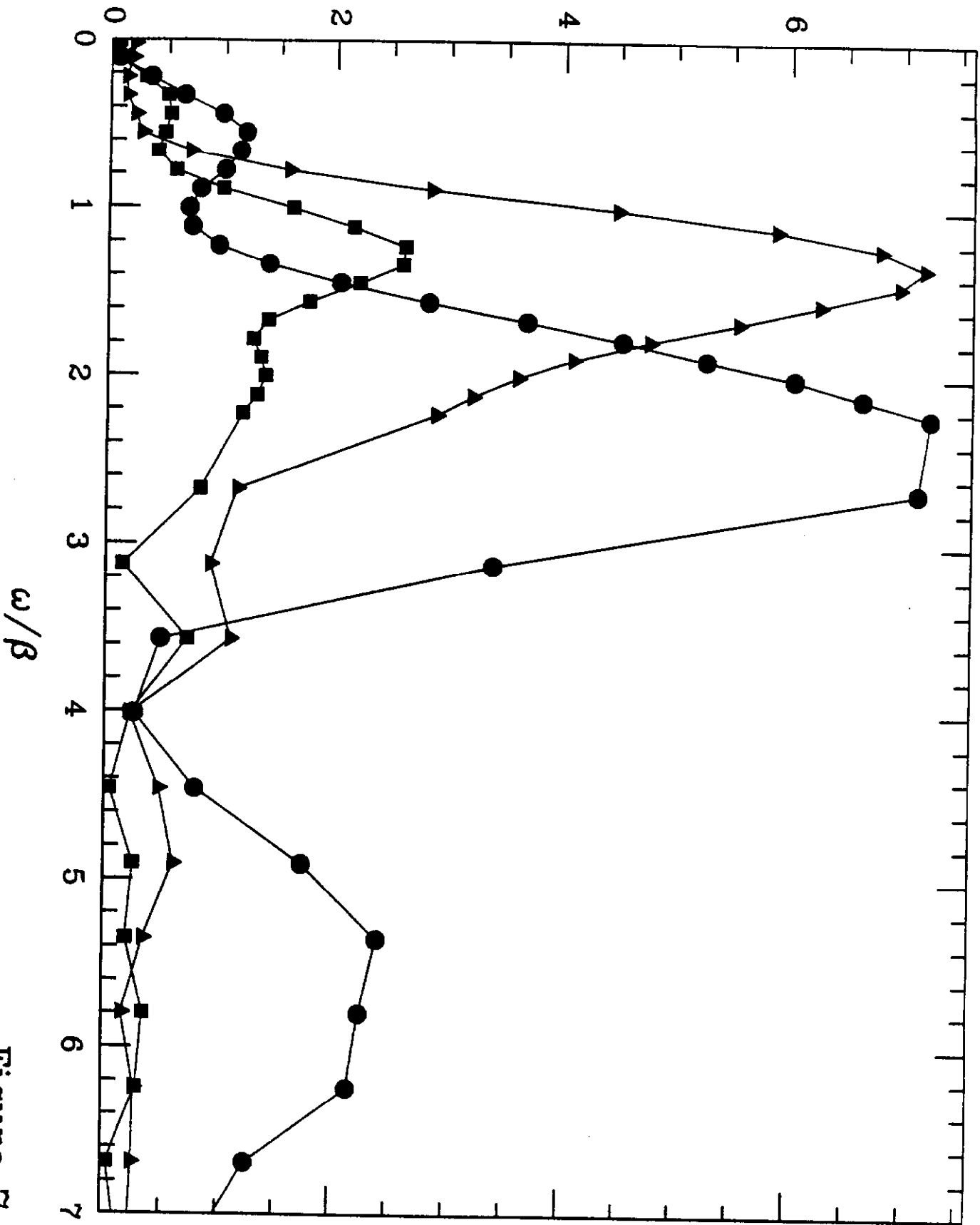


Figure 7

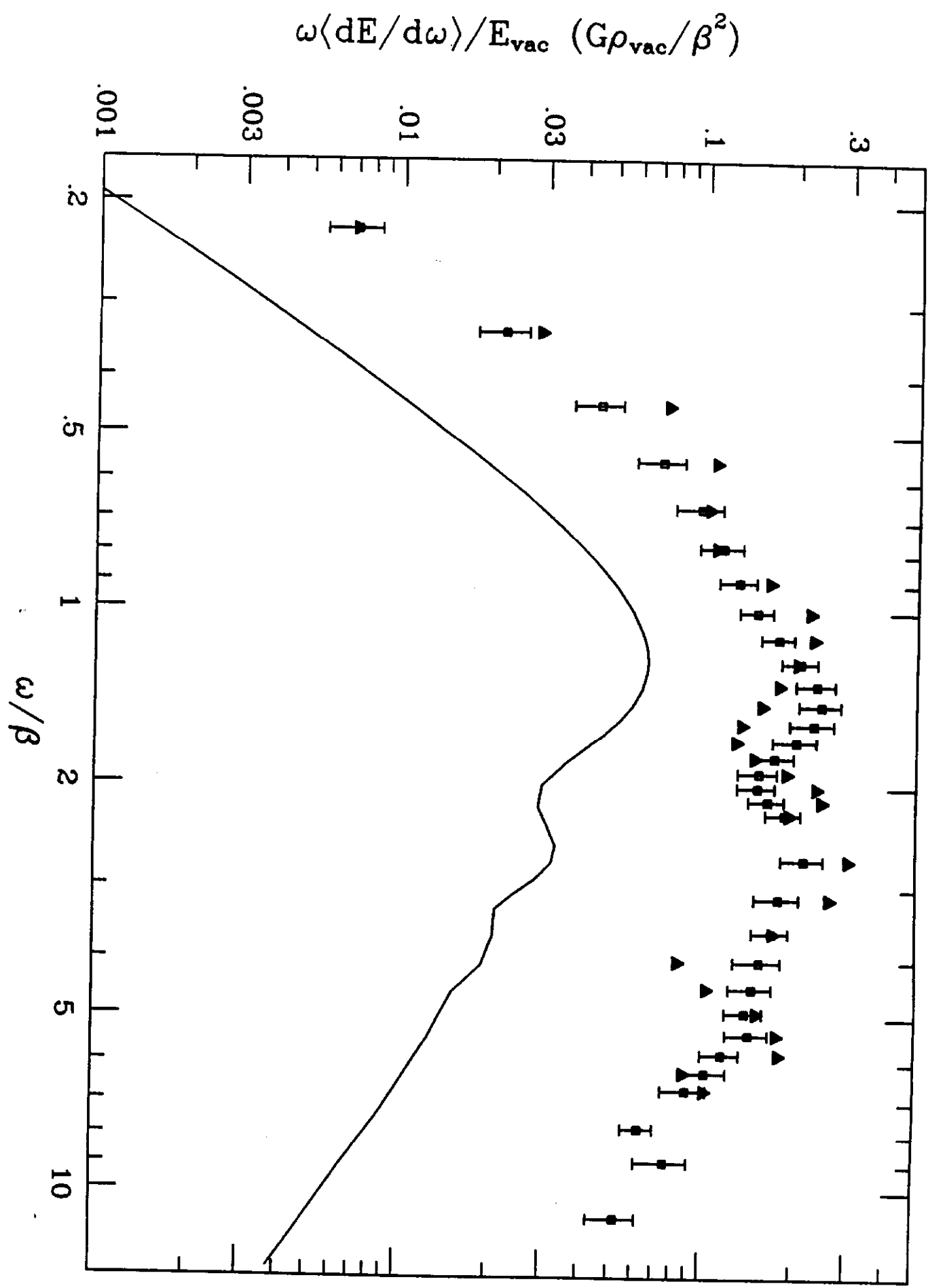


Figure 8

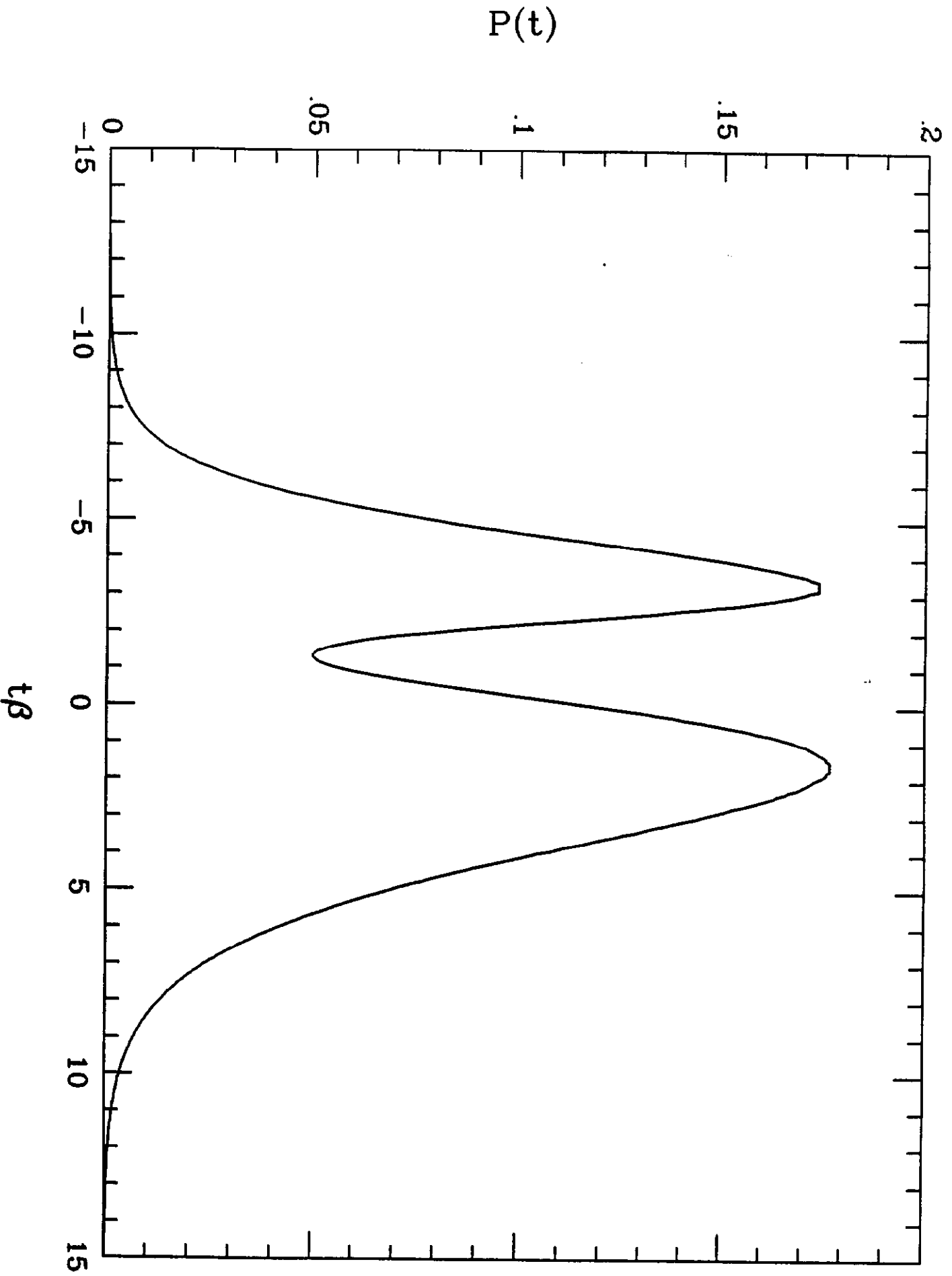


Figure 9

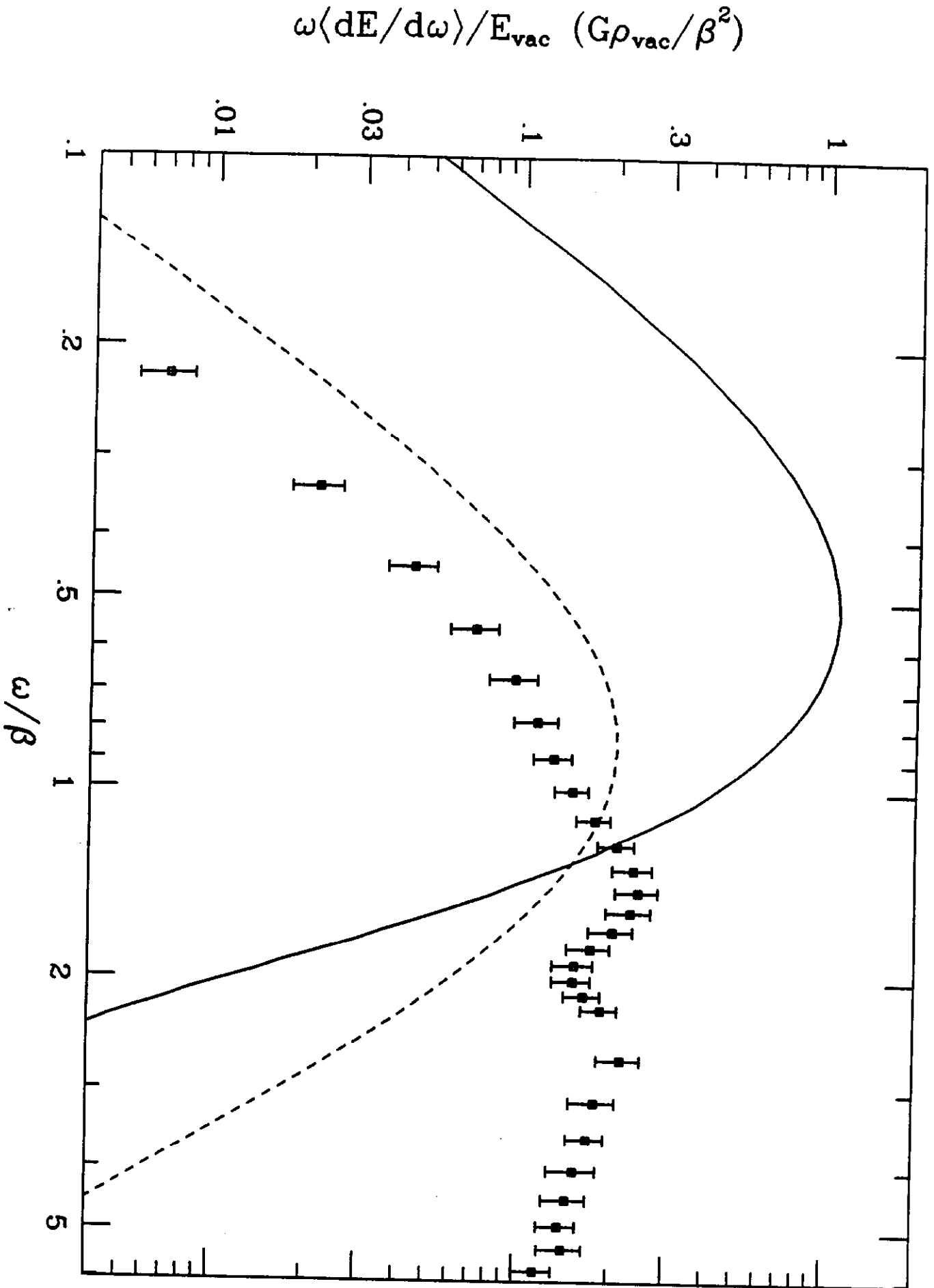


Figure 10

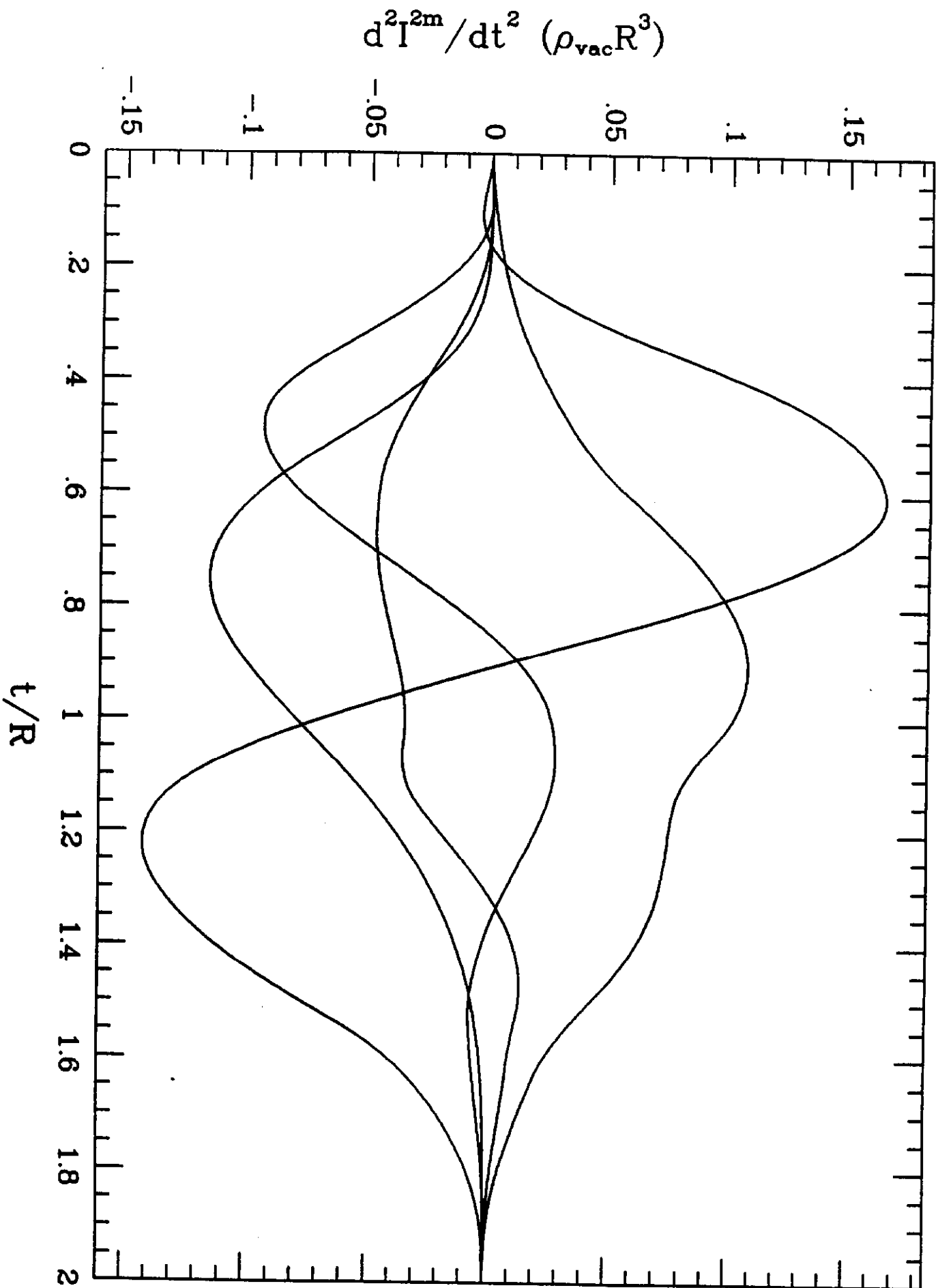


Figure 11 (a)

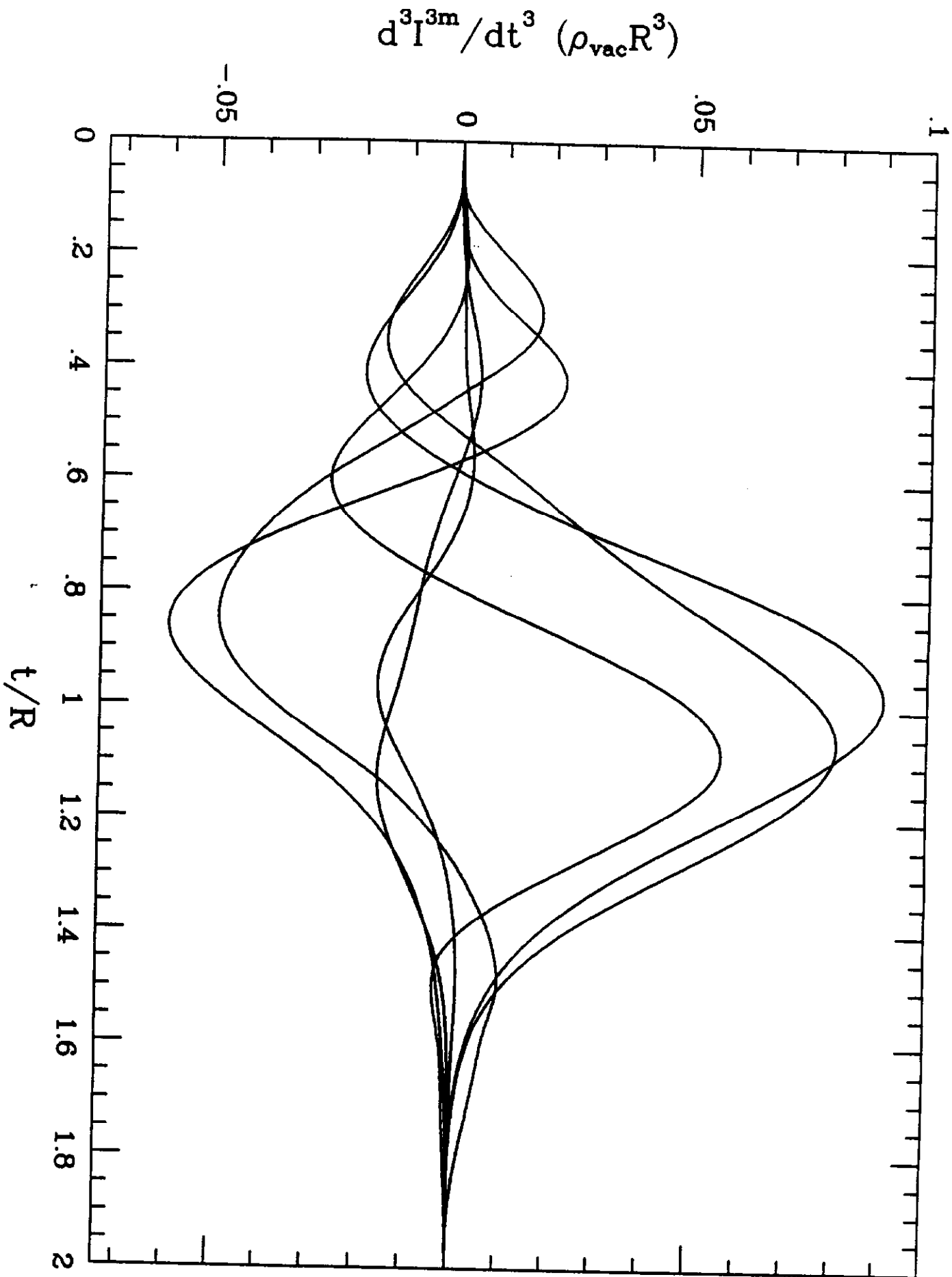


Figure 11 (b)

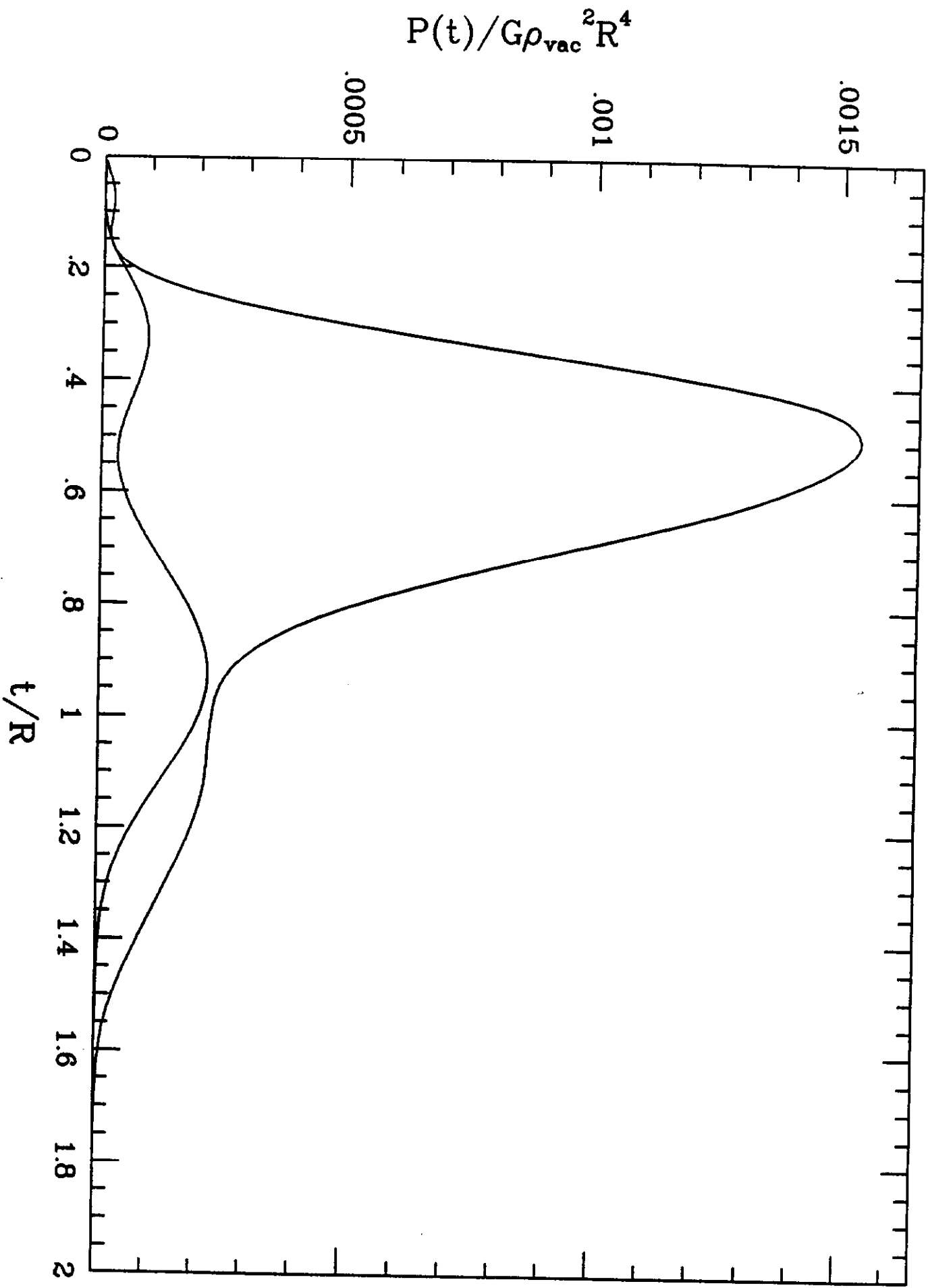


Figure 12

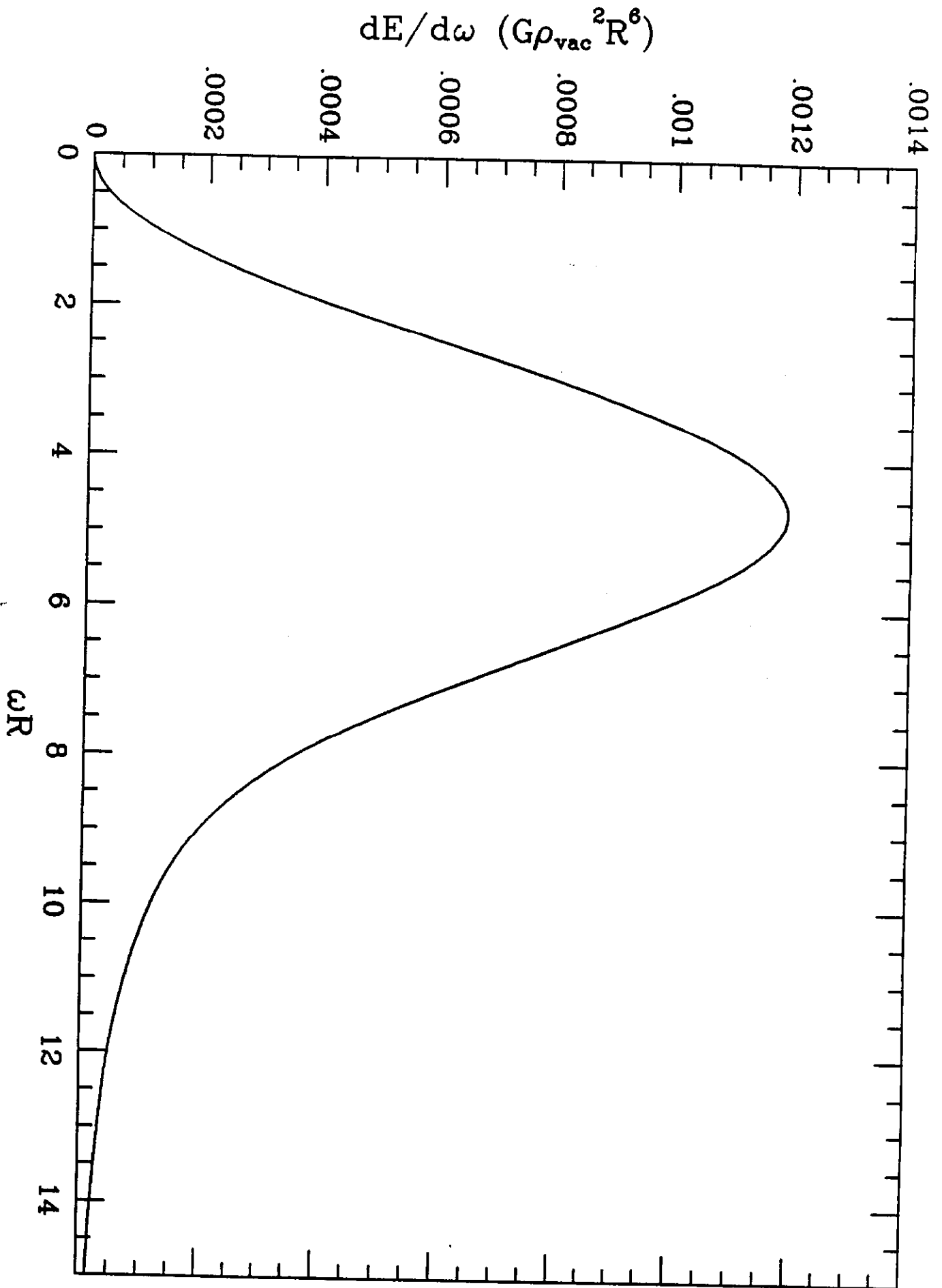


Figure 13